Experimental determination of the rate constants for spin exchange between optically pumped K, Rb, and Cs atoms and ^{129}Xe nuclei in alkali-metal—noble-gas van der Waals molecules

X. Zeng, Z. Wu, T. Call, E. Miron, D. Schreiber, and W. Happer
Department of Physics, Princeton University, Princeton, New Jersey 08544
(Received 28 February 1984)

By analyzing the measured spin-relaxation transients of ^{129}Xe nuclear spins and alkali-metal-atomic spins in mixtures of alkali-metal-atom vapors, Xe gas, and larger amounts of N_2 gas, we have determined the three-body formation rates and the spin-transfer probabilities for alkali-metal—noble-gas van der Waals molecules. Three parameters, in addition to the spin quantum numbers of the alkali-metal and noble-gas nuclei, are needed to predict the spin-transfer rates. These parameters, which we have determined from experimental measurements, are $x=\gamma N/\alpha$, the ratio of the spin-rotation interaction γN to the spin-exchange interaction α; p_0, the third-body pressure for which the molecular breakup rate τ^{-1} is equal to the spin-rotation frequency $\gamma N/h$; and Z, the three-body rate constant for forming van der Waals molecules.

I. INTRODUCTION

In 1960 Carver and Bouchiat[1] first showed that it was possible to transfer angular momentum from optically pumped alkali-metal-atom vapors to the nuclei of ^{3}He gas by spin-exchange collisions. However, the spin-transfer rates were discouragingly slow, and the spin-exchange cross section was estimated[2] to be about 10^{-26} cm^2. In 1978 Grover[3] showed that much faster spin-transfer rates could be obtained from the heavy noble gas ^{129}Xe, and the rates appeared to be consistent with a cross section of 10^{-19} cm^2. Subsequent work by Volk *et al.*[4] showed that much of the spin transfer occurred in loosely bound alkali-metal—noble-gas van der Waals molecules. Bhaskar *et al.*[5] showed that a large part of the alkali-metal-atom spin angular momentum was wasted by being transformed into rotational angular momentum of the alkali—noble-gas pair about each other. A comprehensive theory of the spin-transfer and spin-relaxation processes in alkali—noble-gas systems was developed by Happer *et al.*[6]

Because most of the spin transfer between alkali-metal atoms and heavy noble gases occurs in van der Waals molecules, it is not possible to describe the process with a simple spin-exchange cross section. Three steps are involved in the spin exchange, the formation of a van der Waals molecule in a three-body collision, the evolution of the spins during the lifetime of the van der Waals molecule, and the collisional breakup of the molecule as illustrated in Fig. 1. If the alkali-metal-atom spin polarization is described by a high spin temperature, the rates of change of the small longitudinal spin polarizations $\langle F_z\rangle$ and $\langle K_z\rangle$ of the alkali-metal atoms and noble-gas atoms, respectively, are described by the equations[6]

$$\frac{d}{dt}\langle F_z\rangle=\frac{1}{T_F}[q(F,F)\langle F_z\rangle+q(F,K)\langle K_z\rangle]\,, \tag{1}$$

$$\frac{d}{dt}\langle K_z\rangle=\frac{1}{T_K}[q(K,K)\langle K_z\rangle+q(K,F)\langle F_z\rangle]\,, \tag{2}$$

where $1/T_F$ and $1/T_K$ are the molecular formation rates per alkali-metal atom and noble-gas atom, respectively. The spin-transfer coefficient $|q(F,F)|$ is the probability that the alkali-metal-atom spin polarization will be destroyed during the lifetime of the van der Waals molecule, and the coefficient $q(F,K)$ is the fraction of the nuclear spin of the noble-gas atom which is transferred to the alkali-metal atom during the lifetime of the molecule. The coefficients $q(K,K)$ and $q(K,f)$ have analogous meanings.

The spin-transfer coefficients depend on the product $H\tau$ of the molecular spin interaction Hamiltonian H and the mean, collisionally limited lifetime τ of the molecule.

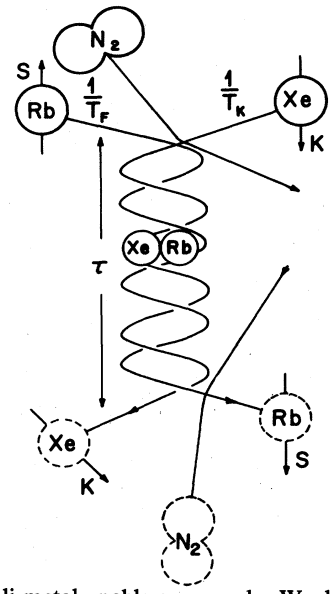

FIG. 1. Alkali-metal—noble-gas van der Waals molecules are formed in three-body collisions at a rate of T_F^{-1} per alkali-metal atom and T_K^{-1} per noble-gas atom. They are broken up at a rate of τ^{-1} by collisions with other atoms or molecules.

That is, by measuring spin-transfer coefficients one cannot distinguish between a weak Hamiltonian acting for a long molecular lifetime and a strong Hamiltonian acting for a short molecular lifetime. Experiments have shown that the simplest spin Hamiltonian consistent with presently known experimental data is[6]

$$H = A\vec{I}\cdot\vec{S} + \gamma\vec{N}\cdot\vec{S} + \alpha\vec{K}\cdot\vec{S}\,, \tag{3}$$

where $A\vec{I}\cdot\vec{S}$, the isotropic magnetic dipole interaction between the nuclear spin $\vec{I}$ and the electron spin $\vec{S}$ of the alkali atom, is similar in magnitude to that of a free alkali-metal atom. The spin-rotation interaction $\gamma\vec{N}\cdot\vec{S}$ is the primary cause of the spin relaxation of alkali-metal atoms in heavy noble gases, and it has been measured for alkali—noble-gas systems in elegant experiments by Bouchiat *et al.*[7] Finally, the isotropic magnetic dipole interaction $\alpha\vec{K}\cdot\vec{S}$ between the nuclear spin $\vec{K}$ of the noble gas and the electron spin $\vec{S}$ of the alkali-metal atom is responsible for spin exchange between the alkali-metal and noble-gas atoms, and theoretical estimates of the magnitude of α have been given by Herman.[2]

The interaction $A\vec{I}\cdot\vec{S}$ is so large compared to the other terms in the Hamiltonian or compared to the natural width $h\tau^{-1}$ of the energy levels under ordinary experimental conditions that $A\vec{I}\cdot\vec{S}$ has no influence on the spin-transfer coefficients and serves only to make $\vec{F}=\vec{I}+\vec{S}$ a good quantum number of the molecule. The spin-tranfer coefficients therefore depend only on the two parameters $\gamma N\tau$ and $\alpha\tau$. We shall find it more convenient to choose the related dimensionless parameters

$$x = \frac{\gamma N}{\alpha} \tag{4}$$

and

$$\phi = \frac{\gamma N\tau}{\hbar} \tag{5}$$

as the independent variables of the spin-transfer coefficients.

The parameter $x=\gamma N/\alpha$ plays the same role in the Hamiltonian (3) as the Breit-Rabi field parameter for the hyperfine structure of the hydrogen atom.[8] Our experiments show that $x^2 \gg 1$ in all alkali—noble-gas systems studied thus far, and it is therefore possible to use x^{-2} as a perturbation expansion parameter in closed-form theoretical expressions for the spin-transfer coefficients. The phase angle ϕ can be thought of as the angle by which the alkali spin $\vec{S}$ would precess about $\vec{N}$ during a molecular lifetime if there were no nuclear spin I to slow down the precession frequency. Since the molecular lifetime is limited by collisions of van der Waals molecules with the gas in the cell, we expect that ϕ will be inversely proportional to the gas pressure p, i.e.,

$$\phi = \frac{p_0}{p}\,, \tag{6}$$

TABLE I. Summary of results of measuring parameters x, p_0, and Z.

Parameter (unit)	Description	Comment	$^{39}K^{129}Xe$	$^{85}Rb^{129}Xe$	$^{87}Rb^{129}Xe$	$^{133}Cs^{129}Xe$
I	Nuclear spin of alkali-metal atom	Slower optical pumping or alkali-metal relaxation rates for large I	$\frac{3}{2}$	$\frac{5}{2}$	$\frac{3}{2}$	$\frac{7}{2}$
K	Nuclear spin of noble-gas atom		$\frac{1}{2}$	$\frac{1}{2}$	$\frac{1}{2}$	$\frac{1}{2}$
x	Breit-Rabi field parameter $x=\frac{\gamma N}{\alpha}$	Determines fractions of alkali-metal atom spin S which are transferred to rotational angular momentum N and noble-gas nuclear spin K	3.5± 0.3	3.2± 0.3	3.2± 0.3	2.9± 0.3
p_0 (Torr)	Characteristic pressure $p_0=p\frac{\gamma N\tau}{h}$	Sets scale for dependence of spin-transfer rates on third-body pressure	105 ±20	103 ± 10	103 ±10	130 ±40
Z (10^{-32} cm^6 sec^{-1})	$Z[M][Xe][N_2]$ molecular formation rate per unit volume	Sets magnitude of spin-transfer rates	5.7± 0.5	5.0± 0.5	5.2± 0.5	5.3±1

where p_0 is a characteristic pressure.

In the experiments described below the sample cells contain 0.5—1 Torr of Xe gas, about 10^{-5} Torr of alkali-metal-atom vapor and 10—100 Torr of N_2 gas. The molecular breakup will almost always be due to a collision with a N_2 molecule and we may therefore identify p in (6) as the third-body (N_2) pressure.

The characteristic pressure will depend on the chemical nature of the van der Waals molecule (i.e., p_0 will not be the same for KXe and RbXe) and we also expect p_0 to depend on the nature of the gas responsible for collisional breakups of the molecule (e.g., we know that p_0 is different for N_2 and He gas).[9] However, we expect p_0 to be the same for van der Waals molecules which differ only in their isotopic composition (i.e., p_0 should be the same for $^{129}Xe^{87}Rb$ and $^{131}Xe^{85}Rb$). In contrast, we expect the Breit-Rabi parameter x to be independent of the gas which causes the collisional breakup of the molecule. We also expect x to be the same for van der Waals molecules containing different isotopes of the alkali-metal atom (i.e., x will be the same for $^{129}Xe^{87}Rb$ and $^{129}Xe^{85}Rb$). However, we expect x to be different for van der Waals molecules containing different isotopes of the noble gas (i.e., we expect different values of x for $^{129}Xe^{85}Rb$ and $^{131}Xe^{85}Rb$, but the values of x should be proportional to the Larmor frequencies of the nuclei of ^{129}Xe and ^{131}Xe).

The molecular formation rates $(T_F)^{-1}$ and $(T_K)^{-1}$ per alkali-metal atom M and per noble-gas atom should be related to the respective number densities $[M]$ and [Xe] by

$$\frac{[M]}{T_F}=\frac{[\mathrm{Xe}]}{T_K}=Z[M][\mathrm{Xe}][\mathrm{N_2}]\,, \tag{7}$$

where $[N_2]$ is the number density of nitrogen molecules which, as we mentioned above, are almost always the third body involved in the formation of van der Waals molecules. We must therefore know the rate constant Z for three-body formation of van der Waals molecules as well as the parameters x and p_o to fully describe the spin-transfer process (1) and (2). All three of these parameters have been measured by methods to be described below, and the results are summarized in Table I.

II. CELL PREPARATION

The sample cells for our experiments are Pyrex glass spheres with an outer diameter of about 30 mm and a wall thickness of about 1 mm. The cells are prepared with a constricted glass stem, and a silicone coating[10] is applied to the interior of the cells by injecting about 2 ml of a 10% solution of "Surfrasil" in cyclohexane into the cell and shaking the cell vigorously. The solution is then removed and the cell interior is rinsed one or two times with pure cyclohexane. The cells are allowed to dry in air for about one day, and they are then sealed onto a 13-mm Pyrex manifold. The seal is made carefully to avoid heating and possible damage to the silicone coating within the sphere, and the completed manifold is not annealed for the same reason. The manifold is attached to a vacuum system as sketched in Fig. 2. A Pyrex U tube with a 1 g ampoule of K metal is inserted between the cells and the pump to serve as a getter for any impurities in the commercial gases used to fill the cell and to limit any contamination due to back streaming from the silicone oil diffusion pump. An open stopcock C is placed between the getter and the cells. Pure alkali metal from a glass ampoule, or alkali chloride salt and calcium metal chips, are placed in a glass retort sealed to the extreme end of the cell manifold. The cells are baked under a vacuum of 10^{-6} Torr at 150°C for 12 h. This seems to do no harm to the silicone coatings. While the cells are cooling down to room temperature the potassium metal getter is flashed with a hand torch so that some 15 cm of the U tube is coated with potassium metal. The alkali metal of interest is then distilled into the cells and the alkali retort is pulled off at the constriction D. The cells are then isolated from the pump by closing the valve V, and the desired amount (usually 1 Torr) of isotopically enriched Xe (69 wt. % ^{129}Xe) (Ref. 11) is admitted to the cells from the stainless-steel lecture bottle B. The gas pressure is read at ~20°C with mechanical billows gauges made by the Wallace Tiernan Company, one with a range of 0—20 Torr and one with a range of 0—800 Torr. The stopcock C is then closed and the xenon gas to the left of the stopcock is frozen back into steel bottle B by immersing the bottle in

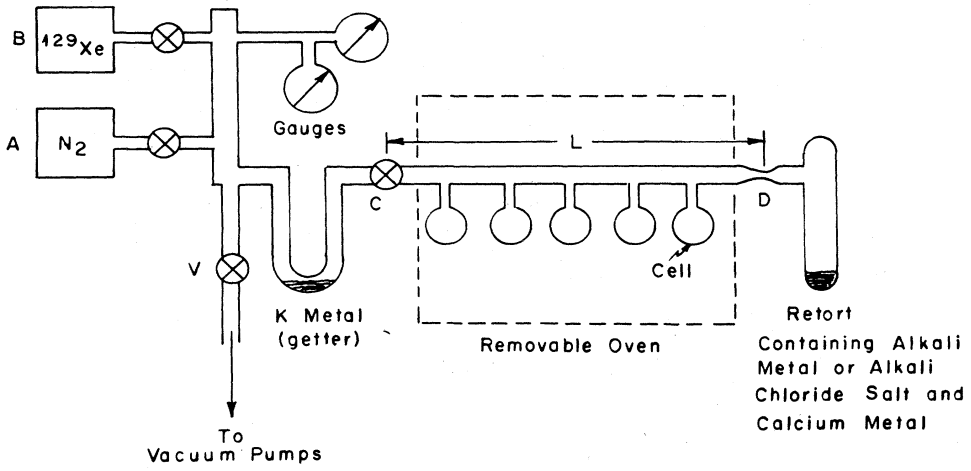

FIG. 2. Vacuum system for filling sample cells. Valve C is used to limit the mixing volume and speed up the interdiffusion of Xe and N_2 gas.

liquid nitrogen. Nitrogen gas is now admitted to the system from a glass bottle A and the desired pressure is obtained by pumping out any excess gas if necessary. The nitrogen pressure is always much larger than the pressure of the Xe to the right of stopcock C. Stopcock C is opened for about one-half second, and nitrogen gas rushes in to equalize the pressure on both sides of stopcock C. Owing to the rapid inflow of N_2 gas, a negligible amount of xenon flows to the left side of stopcock C during the brief time it is open. The glassware to the right of stopcock C now contains the same amount of Xe as before, and it contains the same total pressure, determined from the gauges, as the gas to the left of the closed stopcock C. Ample time must be allowed for the nitrogen and xenon to mix by diffusion, since convective mixing is probably negligible after the initial turbulence of the inflowing N_2 gas has decayed. Before pulling off the cells we allow the elapse of at least five characteristic time intervals

$$\frac{L^2 p(N_2)}{4\pi^2 D_0(760\ \text{Torr})},$$

where $D_0 \cong 0.1\ \text{cm}^2\,\text{sec}^{-1}$ is the diffusion constant of Xe in N_2 gas at a pressure of 760 Torr (one atmosphere) and L is the length of the cell manifold (see Fig. 2).

The cells are wrapped in wet asbestos paper to avoid overheating the silicone-coated interior of the glass sphere during the melting of the glass neck to pull the cells from the manifold. The average cell temperature does not deviate much from room temperature during the sealoff operation.

Before using the cells we are careful to leave about 0.5 cm^2 of alkali metal exposed near the tip of the cell. The interior of the cell also contains minute droplets of alkali metal spread across the surface. These small droplets do not interfere with the optical pumping and they help to ensure that the alkali-metal-atom vapor pressure is close to the saturated vapor pressure at the cell temperature. We have found that the alkali-metal-atom vapor pressure is below the saturated vapor pressure limit if the alkali metal is confined to an extended neck of the cell, or if the cells are not "cured" by being baked at 85 °C for at least three days before use.

III. MEASUREMENT AND ANALYSIS OF SPIN-RELAXATION TRANSIENTS OF ALKALI-METAL ATOMS

In this section we describe our experimental method to measure the spin-relaxation transients of alkali-metal atoms, and we show that the slowest decay rate γ_1 of spin-polarized alkali-metal atoms is mainly due to spin relaxation in alkali-metal—noble-gas van der Waals molecules, i.e.,

$$\gamma_1 = \frac{1}{T_F} |q(F,F)| + \cdots, \tag{8}$$

where $1/T_F$ is the molecular formation rate per alkali-metal atom and $|q(F,F)|$ is the probability that the total angular momentum $\langle F_z \rangle$ of the alkali-metal atom is destroyed during the lifetime of the van der Waals molecule. Relatively small contributions to γ_1 from optical pumping, spatial diffusion, binary collisions, and alkali-metal-atom—alkali-metal-atom spin-exchange collisions are denoted by the centered ellipsis in (8).

The spin relaxation of alkali-metal atoms is substantially more complicated than the nuclear spin relaxation of ^{129}Xe. This is because the number of potentially different longitudinal relaxation times is one less than the number of sublevels for the spin system of interest.[12] Thus, for the spin-$\frac{1}{2}$ nucleus of ^{129}Xe only one longitudinal relaxation time is expected, and indeed our experiments have shown that the spin-relaxation transient of ^{129}Xe is always very well described by a single exponential function of time. On the other hand, experimental studies of spin relaxation in alkali-metal-atom vapors almost always reveal more than one exponential decay. Since there are $2(2I+1)$ spin sublevels of an alkali-metal atom we could have to deal with $4I+1$ different decay rates or 15 decay rates in the case of ^{133}Cs with $I=\frac{7}{2}$. This large number of relaxation times can occur even if the spin Hamiltonian which is responsible for the relaxation is very simple and contains only one interaction, for example, a spin-rotation interaction $\gamma\vec{N}\cdot\vec{S}$. Fortunately, the experimental situation is simplified by two factors. First, no more than five of the $4I+1$ relaxation times can contribute to the optical signal at low magnetic fields.[13,14] Second, under the conditions of our experiments, in particular the occurrence of rapid alkali-metal-atom—alkali-metal-atom spin-exchange collisions, one of the relaxation rates, γ_1, is substantially slower than all of the rest. Our experiments are designed to measure the slowest relaxation rate, and we make no attempt to quantitatively measure any of the faster rates.

As was first shown by Bouchiat *et al.*,[13] five observables can contribute to the polarization-dependent attenuation of D_1 or D_2 light by spin-polarized alkali-metal-atom vapors in weak magnetic fields. There is one monopole observable $\langle \vec{I}\cdot\vec{S} \rangle$, the population imbalance between the Zeeman multiplets a and b; two dipole observables $\langle a_z \rangle$ and $\langle b_z \rangle$; and also two quadrupole observables $\langle 3a_z^2 - a(a+1) \rangle$ and $\langle 3b_z^2 - b(b+1) \rangle$. Because the relaxation processes have an isotropic character at low magnetic fields, the observable $\langle \vec{I}\cdot\vec{S} \rangle$ relaxes with a single exponential decay rate γ_0. The two observables $\langle a_z \rangle$ and $\langle b_z \rangle$ can be coupled to each other by the relaxation process so that their relaxation is characterized by two exponential decay rates γ_1 and γ_1'. Under the conditions of our experiments the rate γ_1 is the slowest of the five observable rates. Similarly, two rates γ_2 and γ_2' contribute to the relaxation of the quadrupole observables.

The apparatus used to measure the alkali-metal-atom spin-relaxation transients is sketched in Fig. 3. A more detailed description of the main components of the apparatus is given in Sec. IV. All of the sample cells contained 1 Torr Xe (69 wt. % ^{129}Xe), alkali metal, and various amounts of N_2 gas. The method is similar to that of Franz,[15] since we observe the time-dependent increase in intensity of circularly polarized light as it passes through an initially unpolarized alkali-metal-atom vapor while the spin polarization is being built up by optical pumping. An example of such an optical-pumping transient is shown in Fig. 4. Before the transient begins, the longitudinal polarizations $\langle a_z \rangle$ and $\langle b_z \rangle$ are maintained equal to zero by a radio-frequency magnetic field which oscillates at the Zeeman resonance frequency, $(2I+1)^{-1}2.8$

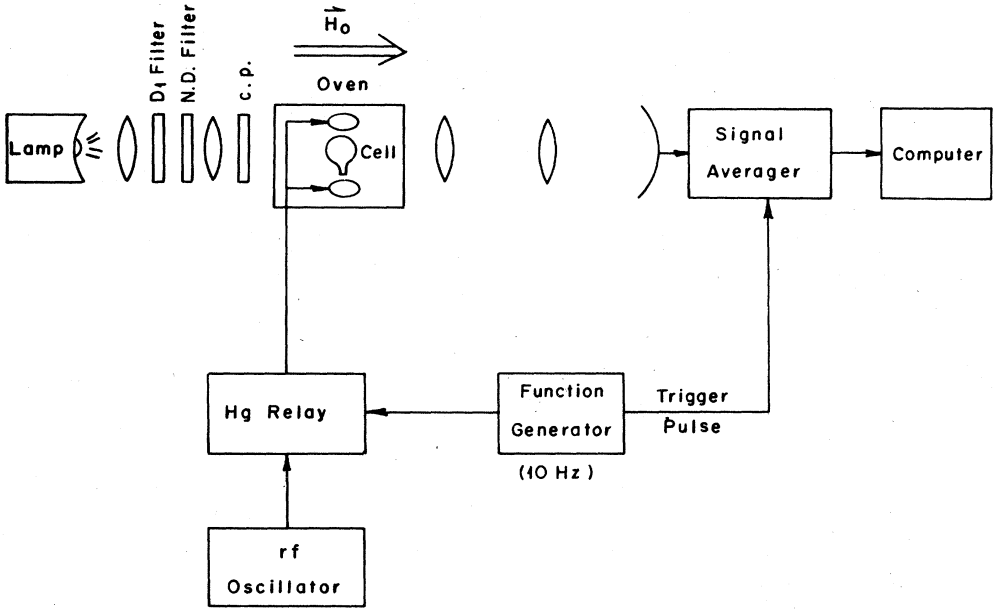

FIG. 3. Apparatus to measure the optical-pumping transients of alkali-metal-atom vapors. The sudden removal of the saturating rf field allows the transparency of the vapor to build up to its steady-state value with several different exponential time constants.

MHz/G of the alkali-metal atoms. The static magnetic field of ~ 6 G is so low that the strong rf field drives the Zeeman transitions in both the upper and lower multiplets to saturation. The transient response of Fig. 4 begins when the rf field is suddenly turned off with the Hg relay. The transients are repetitively generated at a 10 Hz rate and added in a signal averager to build up good signal-to-noise ratios. The longitudinal polarizations build up exponentially to their steady-state, optically pumped values. For example, as a function of time t after the rf is turned off, the dipole polarization evolves according to

$$\langle f_z \rangle = W_{1f}(1-e^{-\gamma_1 t}) + W'_{1f}(1-e^{-\gamma'_1 t}) . \quad (9)$$

Here $f = I \pm \frac{1}{2}$ (a or b) and both $\langle a_z \rangle$ and $\langle b_z \rangle$ evolve with the same decay rates, a slow rate γ_1 and a faster rate γ'_1. The weights W_{1f} and W'_{1f} depend on the details of the relaxation process but W_{1f} will ordinarily be larger than W'_{1f}. Equations similar to (9) hold for the two quadrupole observables and for $\langle \vec{I} \cdot \vec{S} \rangle$, except that only one exponential occurs for $\langle \vec{I} \cdot \vec{S} \rangle$ and the observables may not be zero at $t=0$ since neither $\langle \vec{I} \cdot \vec{S} \rangle$ nor the quadrupole observables are necessarily destroyed by a resonant rf field.

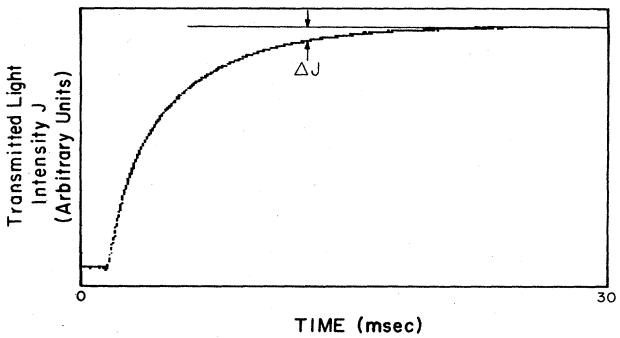

FIG. 4. Example of an optical-pumping transient recorded with the apparatus of Fig. 3. The intensity of the transmitted light increases with time because of the buildup of spin polarization in the vapor as a result of optical pumping.

The intensity J of the transmitted light will be related to the intensity J_0 of the light incident on the sample cell by

$$J = J_0 A , \quad (10)$$

where A is the attenuation of the vapor. We expect A to depend on the spectral profile and polarization of the light, the alkali-metal-atom vapor density, and the five observables $\langle \vec{I} \cdot \vec{S} \rangle$, $\langle a_z \rangle$, $\langle b_z \rangle$, ..., which determine the photon absorption cross section of the alkali-metal atoms. For sufficiently small spin polarization we can always write for $\sigma_\pm$ light

$$A_\pm(\langle a_z \rangle, \langle b_z \rangle, \ldots) = A_0 \pm \langle a_z \rangle \frac{\partial A}{\partial \langle a_z \rangle} \pm \langle b_z \rangle \frac{\partial A}{\partial \langle b_z \rangle} + \cdots . \quad (11)$$

The partial derivatives $\partial A / \partial \langle a_z \rangle$ are to be evaluated at $\langle a_z \rangle = 0$, $\langle b_z \rangle = 0$, etc. They can be calculated in terms of the spectral profile and polarization of the incident light and in terms of the polarization-dependent cross section of the alkali-metal atoms for light absorption.[16] In view of (9) we can write (11) as

$$A = A_0 \pm A_1(1-e^{-\gamma_1 t}) \pm A'_1(1-e^{-\gamma'_1 t}) + \cdots , \quad (12)$$

where the coefficients A_1 and A'_1 can be easily evaluated in terms of the weights W_{1f}, W'_{1f} and the coefficients $\partial A / \partial \langle f_z \rangle$. The difference between the limiting attenuation A_∞ at long times after the start of the transient and the attenuation A at time t is

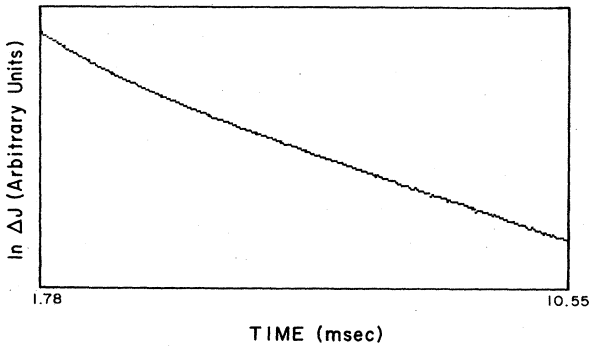

FIG. 5. The difference $\Delta J = J_\infty - J$ between the steady-state light intensity J_∞ and the transient light intensity J decays with several exponentials; the slowest exponential has a particularly simple significance.

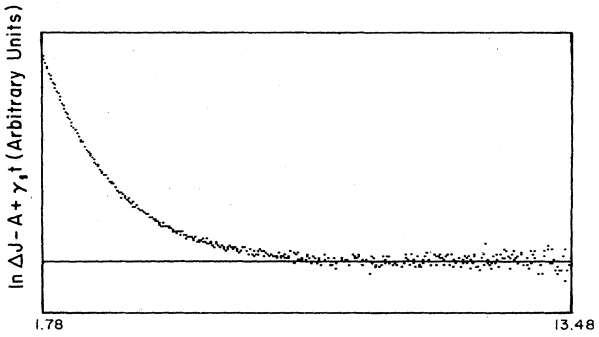

FIG. 6. Residuals for a fit to the slowest exponential of data like those of Fig. 5.

$$\Delta A = A_\infty - A = A_1 e^{-\gamma_1 t} + A_1' e^{-\gamma_1' t} + \cdots . \tag{13}$$

For times longer than a few units of $(\gamma_1' - \gamma_1)^{-1}$ we may ignore all but the slowest transient in (13) and use (10) to write the observed transient as

$$\Delta J \simeq J_0 A_1 e^{-\gamma_1 t} \text{ for } t \gg (\gamma_1' - \gamma_1)^{-1} . \tag{14}$$

Thus in our experiments we measure ΔJ as a function of time and we identify the limiting slope of $\ln \Delta J$ at large times as the slow decay constant $-\gamma_1$. An example of a measured value of $\ln \Delta J$ versus t is shown in Fig. 5. In Fig. 6 we show the residuals for linear fit to the data of Fig. 5. From Fig. 6 we see that there is negligible contribution of the faster exponentials to the decay transient after about 6 msec.

Both experimental measurements and theory show that γ_1 is an increasing function of the pumping-light intensity J. For sufficiently weak light we expect to find a linear dependence on J,

$$\gamma_1(J) = \gamma_{10} + J \left[\frac{\partial \gamma}{\partial J} \right] + \cdots , \tag{15}$$

with the partial derivative evaluated at $J = 0$. In Fig. 7 we show an example of an experimental measurement of γ_1 versus J. The effect of the pumping light is relatively small and we may obtain γ_{10}, the slowest relaxation rate in the dark, by extrapolating γ_1 back to zero light intensity.

Using formulas from Ref. 17, Hou *et al.*[18] have shown that the decay rate of the slowest transient is expected to be

$$\gamma_{10} = r_1 + \frac{(2I+1)^2+2}{2(2I+1)^2} r_2 + \frac{1}{3T_{ex}} \frac{(2I+1)^2+2}{(2I+1)^2} - \frac{1}{2} \left[\left[\frac{2}{3T_{ex}} \frac{[(2I+1)^2+2]}{(2I+1)^2} \right]^2 + \frac{4r_2}{3T_{ex}} \left[\frac{(2I+1)^4 - 2(2I+1)^2 + 4}{(2I+1)^4} \right] + \left[r_2 \frac{(2I+1)^2 - 2}{(2I+1)^2} \right]^2 \right]^{1/2} . \tag{16}$$

There are three characteristic rates in (16). The fastest, the alkali-metal-atom—alkali-metal-atom spin-exchange rate, is expected to be on the order of[19,20]

$$\frac{1}{T_{ex}} \sim 10^{-9} [M] \text{ cm}^3 \text{ sec}^{-1} , \tag{17}$$

where $[M]$ is the alkali-metal number density. Representative values of $[M]$ in our work are 5×10^{11} cm^{-3}, so we expect to find values of $1/T_{ex}$ on the order of 500 sec^{-1}. It is interesting to note that (16) becomes independent of $1/T_{ex}$ in the limit $1/T_{ex} \to \infty$. The second characteristic rate is r_2, the electron randomization rate. This refers to a relaxation process which destroys the electron-spin polarization $\langle S_z \rangle$ without affecting the nuclear-spin polarization $\langle I_z \rangle$. In our work we expect electron randomization to be associated with sudden binary collisions between alkali-metal atoms and Xe atoms or N_2 molecules. Alkali-metal-atom—alkali-metal-atom collisions also lead to electron randomization at a rate which has been measured in Cs vapor to be about 1% of the spin-exchange rate.[21] Thus, for Cs-Cs collisions we expect a contribution to r_2 on the order of 5 sec^{-1}, a negligible amount. It is reasonable to expect negligible contributions to r_2 from alkali-metal-atom—alkali-metal-atom collisions in Rb and K vapors also. The contribution of Rb-N_2 collisions to r_2 has been measured by Franz[22] to be 0.145 sec^{-1} per Torr of N_2 gas. Thus, even at the highest N_2 pressure (100 Torr) used in our experiments the contribution Rb-N_2 collisions make to r_2 will only be approximately 14.5 sec^{-1}, a negligible amount. It is reasonable to expect a negligible contribution to r_2 from similar N_2 pressures for Cs and K spin relaxation also.

The electron randomization rate due to binary collisions of alkali-metal atoms with Xe gas is expected to be given

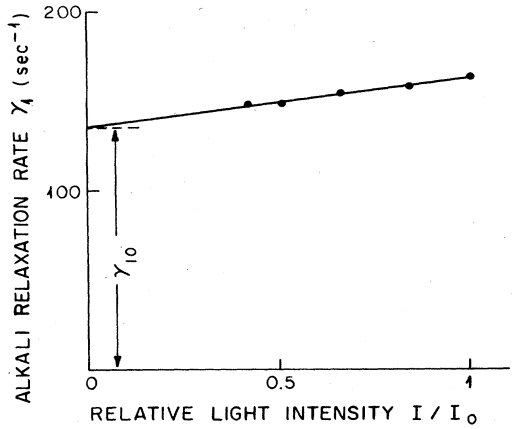

FIG. 7. Dependence of the slowest decay rate γ_1 on the intensity of the pumping light. The light-independent decay rate γ_{10} is obtained by extrapolating the rate to the limit of zero light intensity.

by the formula[6]

$$r_2=\frac{1}{T_{FB}}\left[\frac{2}{3}\left[\frac{\gamma N\tau_B}{\hbar}\right]^2+\frac{2}{3}K(K+1)\left[\frac{\alpha\tau_B}{\hbar}\right]^2 f\right], \quad (18)$$

where T_{FB}^{-1} is the rate of binary collisions per alkali-metal atom, and τ_B is an appropriately defined duration of a binary collision. The fraction of ^{129}Xe atoms in the isotopically enriched sample is f, and we may ignore the fraction of ^{131}Xe, the other isotope with nonzero nuclear spin, because it is much less abundant in our gas samples and because the term in (18) proportional to α^2 is about a factor of 2 smaller for ^{131}Xe than for ^{129}Xe for equal isotopic fractions as a result of the different spins and nuclear moments of the two isotopes.

The electron randomization rate due to binary collisions of alkali-metal atoms with Xe gas has been measured in two instances. For RbXe Bouchiat *et al.*[7] report

$$r_2(\text{RbXe})=185\ \text{sec}^{-1}\text{Torr}^{-1}p(\text{Xe}), \quad (19)$$

while for NaXe Bhaskar *et al.*[23] report

$$r_2(\text{NaXe})=266\ \text{sec}^{-1}\text{Torr}^{-1}p(\text{Xe}). \quad (20)$$

Unfortunately, there seem to be no measurements of the corresponding rates for KXe and CsXe.

The contribution of r_2 to γ_{10} depends on the relative size of r_2 and the spin-exchange rate $1/T_{ex}$ as demonstrated by Hou *et al.*[18] In the limit $1/r_2T_{ex}\to\infty$, Eq. (16) reduces to

$$\gamma_{10}=r_1+\frac{3r_2}{(2I+1)^2+2}, \quad (21)$$

while in the opposite extreme $1/r_2T_{ex}\to 0$, Eq. (16) becomes

$$\gamma_{10}=r_1+\frac{2r_2}{(2I+1)^2}. \quad (22)$$

In both cases there is a substantial slowing-down factor due to the nuclear spin I which is not destroyed in the electron randomizing collision and which therefore regenerates much of the electron-spin polarization after the collision is over. We note that in the limit $1/T_{ex}\to 0$ the eigenobservable associated with γ_{10} was shown by Bouchiat *et al.*[13] to be I_z (or more precisely the sum of the projections of I_z in the upper and lower Zeeman multiplets). In the other limit, where $1/T_{ex}\to\infty$ the eigenobservable[12] is simply F_z, the total spin angular momentum of the alkali-metal-atom vapor. Our experiments on spin relaxation in the alkali-metal-atom vapors are ordinarily done at an alkali-metal number density which corresponds to $1/r_2T_{ex}\gtrsim 3$. This leads to a slowing-down factor which is closer to (21) than (22), and for simplicity we shall use (21) to correct our data. In the case of ^{87}Rb the numerical value of the correction is $r_2/8\simeq 23\ \text{sec}^{-1}$ if we use formula (22) and $r_2/6\simeq 30\ \text{sec}^{-1}$ if we use formula (21). Since both corrections are comparable to the error in the experimental measurements there is little to be gained from choosing a more precise intermediate value. We shall also make the simplifying assumption that the electron ran-

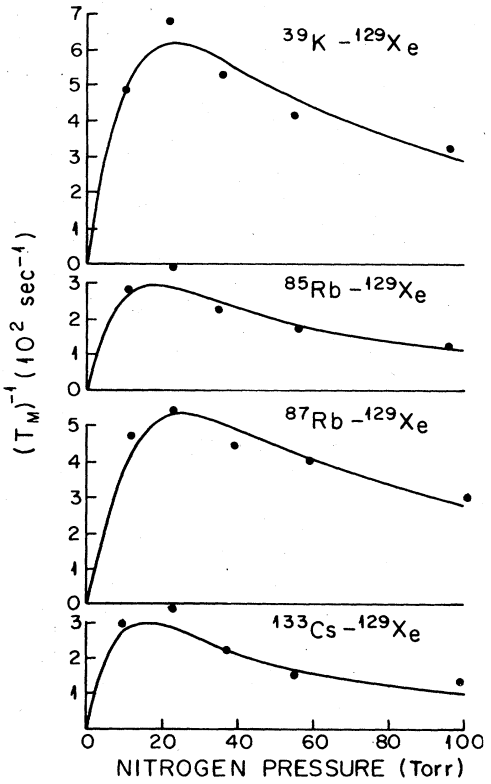

FIG. 8. Summary of the experimentally determined molecular contribution $(T_M)^{-1}$ to the slowest decay rate γ_1 of alkali-metal-atom spins. All cells contained 1 Torr of Xe gas (60 wt. % ^{129}Xe). Small contributions to γ_1 from the pumping light, diffusion to the cell walls, and electron-randomizing binary collisions have been subtracted from γ_1 to obtain $(T_M)^{-1}$ [see Eq. (28)]. Solid curves are $|q(F,F)|T_F^{-1}$ with a distribution of the rotational angular momentum N taken into account. Note that the nuclear spin of the alkali-metal atom causes a substantial slowing down of the alkali-metal decay rates so that the decay rates of ^{85}Rb and ^{87}Rb differ by nearly a factor of 2. These data are used to determine the parameters $(T_F)^{-1}$ and p_0.

domization rates of K and Cs atoms in xenon are the same as for Rb in xenon.

Since the contributions of electron randomization r_2 and spin exchange $1/T_{ex}$ to (16) are small compared to the measured magnitude of γ_{10} (see Fig. 8), we conclude that the dominant contribution to γ_{10} comes from r_1, the third and simplest characteristic rate in (16). The rate r_1 describes those relaxation processes which cause $\langle a_z \rangle$ and $\langle b_z \rangle$ to decay at the rate r_1 with no coupling of $\langle a_z \rangle$ to $\langle b_z \rangle$, i.e.,

$$\frac{d}{dt}\langle f_z \rangle = -r_1 \langle f_z \rangle \ , \tag{23}$$

where $f = a$ or b. An obvious contributor to r_1 is the diffusion of spin polarized alkali-metal atoms to the cell walls. The silicone coatings which are so effective in slowing down the spin relaxation of ^{129}Xe nuclei cause no measurable slowing down of the alkali-metal-atom spin relaxation, probably because we leave the inner walls of the cells coated with many small droplets of alkali metal to try to ensure that the equilibrium saturated vapor pressure of alkali-metal atoms prevails within the cell at a given temperature. The lowest diffusion mode of a sphere of radius R with disorienting walls has a relaxation rate[24]

$$\gamma_D = \frac{\pi^2 D_0}{R^2}\frac{760}{p} \ , \tag{24}$$

where p is the pressure in Torr of the gas (N_2) through which the alkali-metal atoms diffuse and D_0 is the diffusion constant of the gas at one atmosphere (760 Torr). We have measured D_0 for Rb in N_2 and we find

$$D_0(\mathrm{RbN_2}) = 0.20 \ \mathrm{cm^2\,sec^{-1}} \tag{25}$$

at 70°C. This is in satisfactory agreement with the value D_0 ($\mathrm{RbN_2}$) = 0.16 $\mathrm{cm^2\,sec^{-1}}$ at 32°C measured by Franz.[22] For our cells, which have radii of about 13 mm, the diffusion rates γ_D for cells with the lowest N_2 pressures ($\sim$10 Torr) do not exceed 50 $\mathrm{sec^{-1}}$, a relatively small contribution to γ_{10}.

The most important contribution to r_1 and to γ_{10} is relaxation due to the formation of alkali-metal—noble-gas van der Waals molecules. As we already mentioned in connection with (1) and (2) the molecule-induced rate is the product of a formation rate per alkali-metal atom T_F^{-1} and a spin destruction probability $|q(F,F)|$ per molecular lifetime. At high N_2 pressures where $\phi/(2I+1) \ll 1$ one can show that[6]

$$|q(F,F)| = \frac{2}{3}\left[\frac{\phi}{2I+1}\right]^2\left[1+\frac{K(K+1)}{x^2}f\right] \tag{26}$$

where f is the isotopic fraction of ^{129}Xe. There is no restriction on the magnitude of the Breit-Rabi parameter x in (26). For lower N_2 pressures where $\phi/(2I+1) \gtrsim 1$, we may write $|q(F,F)|$ as a power series in x^{-2} and find[6]

$$q(F,F)| = \frac{2}{3}\frac{\left[\frac{\phi}{2I+1}\right]^2}{1+\left[\frac{\phi}{2I+1}\right]^2} + \frac{2K(K+1)f}{9x^2}\frac{\left[3-\left[\frac{\phi}{2I+1}\right]^2\right]}{\left[1+\left[\frac{\phi}{2I+1}\right]^2\right]^3}\left[\frac{\phi}{2I+1}\right]^2$$
$$+\frac{K(K+1)f}{3x^2(2I+1)[I(I+1)+\frac{3}{4}]}\sum_{m_f}\frac{m_f^2\left[\frac{\phi m_f}{x(2I+1)}\right]^2}{1+\left[\frac{\phi m_f}{x(2I+1)}\right]^2} \ . \tag{27}$$

Formula (27) is valid only if $x^2 \gg 1$.

We studied the effects of cell temperature on the slowest decay rate γ_{10} described above and we found that in the case of ^{87}Rb, γ_{10} was independent of cell temperatures in the range of 50 to 80°C to within the $\sim$10% accuracy of the measurements. The main effect of increasing the cell temperature was to increase the weights of the faster relaxation transients shown in Figs. 5 and 6 and to increase the influence of the pumping light on the slowest decay rate; i.e., the slope of the plots like those of Fig. 7 were less at higher cell temperatures, These observations suggest that neither alkali-metal-atom—alkali-metal-atom spin-exchange collisions nor higher-order spatial diffusion modes had any significant effects on the measured value of the slowest relaxation rate γ_1.

In summary, we attribute most of the measured slow decay rate γ_1 to relaxation in alkali-metal—noble-gas van der Waals molecules. To extract the best estimate of the molecular contribution, we make three relatively small corrections to the raw data.

(1) We extrapolate the measured slowest decay rate γ_1 to zero probing light intensity, as shown in Fig. 7, to obtain slowest decay rate γ_{10} for relaxation in the dark.

(2) We subtract from γ_{10} an estimate (24) of the contribution of spatial diffusion of spin polarized alkali-metal atoms to the depolarizing walls of the cell.

(3) We also subtract an estimate of the contribution of electron randomizing collisions between spin polarized alkali-metal atoms and Xe atoms. Since the electron randomization rate has only been measured for Rb and Na, we approximate the rates for K and Cs by the rate (19) for Rb.

Our best estimate for the contribution of van der Waals molecules to the slowest spin-relaxation rate of alkali-

metal atoms is thus

$$\frac{1}{T_M}=\gamma_{10}-\frac{\pi^2 D_0}{R^2}\frac{760}{p}-\frac{3r_2}{(2I+1)^2+2}\ . \tag{28}$$

In Fig. 8 we summarize measured spin-relaxation rates of alkali-metal atoms in 1 Torr of Xe gas (69 wt.% ^{129}Xe), corrected for diffusion and binary collisions according to the right-hand side of Eq. (28). The solid curves are the theoretical value $|q(F,F)|\,T_F^{-1}$ for the relaxation due to van der Waals molecules. Theoretical curves were fit to the data by using the molecular formation rate T_F^{-1} per alkali-metal atom and the characteristic pressure p_0 of (6) as free parameters. The curves are not very sensitive to the Breit-Rabi parameter x and the value of x was not a free parameter in the fits of Fig. 8, but x was instead determined, as described in Sec. V, from the ratio of the ^{129}Xe and alkali-metal-atom spin relaxation rates at higher third-body pressures. The values of $q(F,F)$ used to fit the data of Fig. 8 are about 12% smaller than the value given by Eq. (27) because we averaged the spin-transfer coefficient over a distribution of rotational angular momenta N as described in Ref. 6.

IV. MEASUREMENT AND ANALYSIS OF SPIN-RELAXATION TRANSIENTS OF ^{129}Xe NUCLEI

The relaxation of ^{129}Xe nuclei is relatively simple compared to the spin relaxation of alkali-metal atoms discussed in Sec. III. Since the nuclear spin of ^{129}Xe is $K=\frac{1}{2}$ there can only be one longitudinal relaxation time and our experiments show that the ^{129}Xe transients are well described by a single exponential decay curve instead of a superposition of several exponential decay curves as is observed for spin relaxation of the alkali-metal atoms.

The experimental apparatus for observing the relaxation of the ^{129}Xe spins is shown in Fig. 9. A dc magnetic field ($H_0\approx 5$ G) which is produced by large coils (not shown in Fig. 9) defines the Larmor frequencies of alkali-metal atoms and ^{129}Xe nuclei and lessens the sensitivity of the system to stray magnetic fields. The cell is heated by a stream of hot air and the gas mixture in it is optically pumped by an alkali-metal-atom vapor resonance lamp using a circular polarizer (CP) and a filter which transmits the $D1$ line. During the probe phase of the experiment the circular polarizer is removed and the small amount of elliptical polarization introduced in the unpolarized light by the polarized alkali-metal atoms is detected with a photoelastic modulator. The signal is proportional to the number density of the spin polarized ^{129}Xe nuclei since the short-lived (≈ 1 msec) polarized ^{87}Rb atoms are produced by spin exchange with the xenon. Small amounts of stray elliptical polarization caused by the lamp itself and by the optical components are initially compensated by a rotatable $\lambda/4$ plate. The stray components of the elliptical polarization are temperature sensitive. This leads to a slow, unpredictable drift in the elliptical background polarization during the long ($\approx\frac{1}{2}$ h) relaxation time. To compensate for the slow drift we perform adiabatic rapid passage, i.e., we periodically invert the ^{129}Xe nuclear polarization with a chirped audio-frequency magnetic field which is applied to the small coils. The frequency is swept from 3 to 7 kHz through the ^{129}Xe magnetic resonance of 5 kHz. The xenon polarization is determined by subtracting the average signals during the 5-sec intervals before and after an inversion. This procedure is equivalent to transforming the signal power to higher frequencies and it substantially attenuates noise components with periods longer than 10 sec. An Apple II + computer controls the inversion rates and performs on-line data processing. The signal amplitude is given by $A(t)=A(0)(\epsilon-1)^n\exp(-\tau/\theta)$, where ϵ is the decay per inversion, n is the number of inversions which have occurred by time t, and θ is the ^{129}Xe relaxation time. Variation of the interval betweeen consecutive inversions permits the determination of both θ and ϵ from the decay curve. Independent measurements of θ under the same conditions have a variance from their mean of $\approx 5\%$. Typical decay curves of ^{129}Xe in ^{39}K, ^{85}Rb, and ^{133}Cs alkali-metal-atom vapors are shown in Fig. 10. The decay rate of the ^{129}Xe nuclear polarization θ^{-1} results from the combined effects of the alkali-metal-induced rate

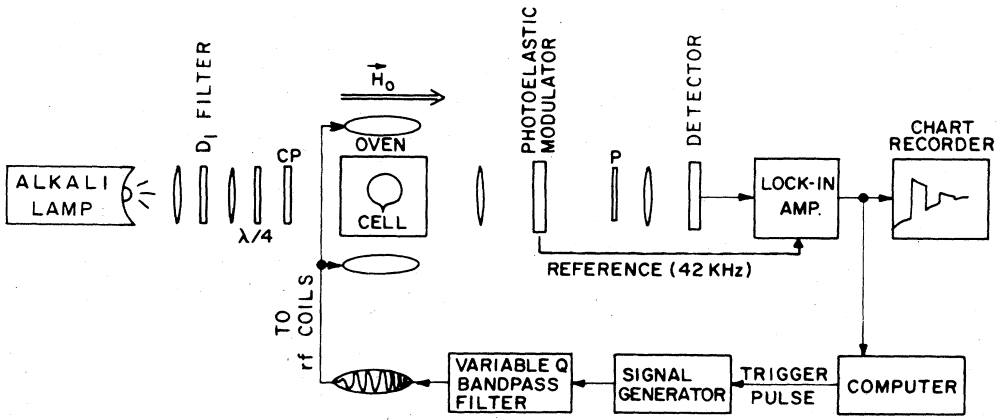

FIG. 9. Apparatus to measure the nuclear-spin relaxation transients of ^{129}Xe in various alkali-metal-atom vapors and in the presence of various amounts of N_2 gas. The ^{129}Xe nuclear polarization is inverted with a chirped audio-frequency pulse from time to time to eliminate slow drifts from the recording system.

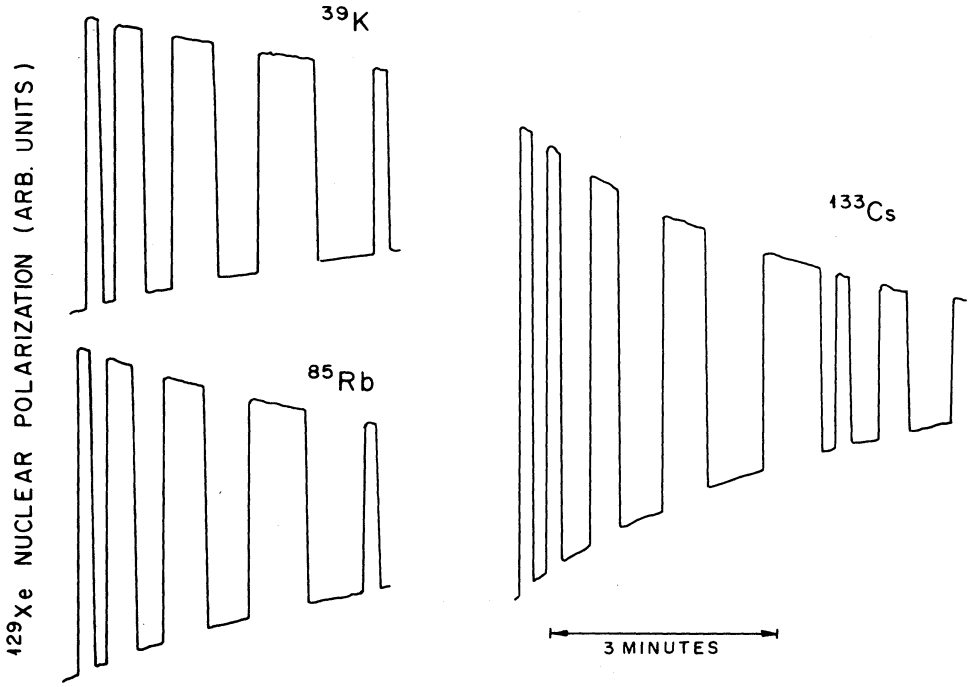

FIG. 10. Representative ^{129}Xe nuclear-spin relaxation transients in ^{39}K, ^{85}Rb, and ^{133}Cs alkali-metal-atom vapors as observed with the apparatus of Fig. 9.

θ_0^{-1} and wall relaxation rate T_w^{-1},

$$\theta^{-1}=\theta_0^{-1}+T_w^{-1}=C[\mathrm{Rb}]+T_w^{-1}\ , \tag{29}$$

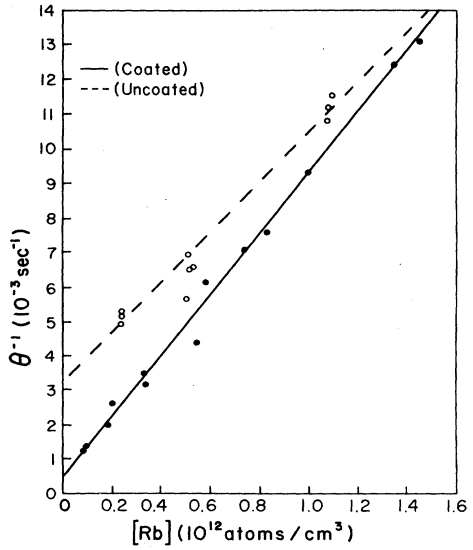

FIG. 11. Dependence of the ^{129}Xe spin-relaxation rate on the ^{87}Rb number density in an uncoated Pyrex cell containing 21 Torr of N^2 gas and in a silicone-coated Pyrex cell containing 14.9 Torr of N_2. Both cells contain 0.5 Torr of Xe, enriched to 69 wt. % isotopic fraction of ^{129}Xe. The wall-induced relaxation rate is the intercept at [Rb]=0. Silicone-coated cells have much longer wall-relaxation times for ^{129}Xe than uncoated cells. The Rb-induced contribution to the ^{129}Xe relaxation rate depends on the third-body (i.e., N_2) gas pressure.

where C and T_w^{-1} are temperature-independent constants. The quantities C and T_w^{-1} are determined by measuring θ^{-1} at various temperatures as shown in Fig. 11. The alkali-metal density is deduced from the measurement of the cell temperature with a nonmagnetic thermocouple and by using empirical saturated vapor-pressure curves for the alkali metals. We should mention that several pieces of evidence have convinced us that the Rb vapor-pressure curve given by Smithells[25] and used by us[5,9,10,30] and by the group at Litton Industries[3,4] to interpret spin-relaxation measurements of xenon isotopes in Rb vapor is incorrect and gives a vapor pressure which is more than a factor of 2 smaller than the true vapor pressure. Bouchiat and Brossel[26] have already commented on this discrepancy. The best data for Rb seem to be those of Killian,[27] whose empirical formula for the saturated vapor pressure of Rb metal, in dyn/cm^2, is

$$\log_{10}p=10.55-4132/T\ . \tag{30}$$

Faraday rotation measurements in our laboratory have shown that the K vapor pressure in our cells for the temperature range 70 to 110 °C is adequately represented by a variant of Killian's[27] formula

$$\log_{10}p=11.57-4964/T\ . \tag{31}$$

Here T is the absolute temperature in Kelvin. For Cs we used the formula tabulated by Nesmeyanov[28] for the saturated vapor pressure in Torr (1 Torr=1333.22 dyn/cm^2):

$$\log_{10}p=11.0531-1.35\log_{10}T-4041/T\ . \tag{32}$$

There is good evidence[29] that the wall-induced rate is a

decreasing function of the cell temperature in the case of ^{131}Xe. In our experiments with ^{129}Xe, the wall-induced rate is so small compared to the alkali-metal-induced rate that any temperature dependence of $1/T_w$ will introduce a negligible error in our inferred values of the alkali-metal-induced rate $C[M]$. We believe that there are two contributions to the alkali-metal-induced rate:

$$C[M]=\frac{1}{\theta_0}=\frac{1}{T_K}|q(K,K)|+\frac{1}{T_{KB}}\frac{1}{2}\left[\frac{\alpha\tau_B}{\hbar}\right]^2. \quad (33)$$

The relaxation due to alkali-metal—noble-gas van der Waals molecules is the product of a molecular formation rate T_K^{-1} per noble-gas atom and a probability $|q(K,K)|$ that the nuclear spin is destroyed during the molecular lifetime. The last term in (33) describes the relaxation due to binary alkali-metal—noble-gas collisions where T_{KB}^{-1} is the rate of binary collisions per noble-gas atom and τ_B is an appropriately defined mean duration of the binary collision.

Several pieces of evidence show that the contribution from binary collisions is small compared to the contribution from van der Waals molecules. First, the binary contribution should be independent of the third-body (nitrogen) pressure, but all of our data show a strong dependence of the ^{129}Xe relaxation rates on the nitrogen pressure. Second, the binary rate should be independent of magnetic fields less than 10^6 G. Measurements by Bhaskar *et al.*[31] have shown that the relaxation rate of ^{129}Xe in Rb is nearly eliminated by an external magnetic field of 200 G.

We may estimate the contribution of binary collisions to the nuclear-spin relaxation of ^{129}Xe by noting that the binary-collision rate T_{KB}^{-1} of (33) is related to the binary-collision rate per alkali-metal atom T_{FB}^{-1} of (18) by

$$\frac{[M]}{T_{FB}}=\frac{[\mathrm{Xe}]}{T_{KB}}. \quad (34)$$

Substituting (18) and (34) into (33) we find that we may write the binary contribution as

$$\frac{1}{\theta_B}=\frac{1}{T_{KB}}\frac{1}{2}\left[\frac{\alpha\tau_B}{\hbar}\right]^2=r_2\frac{[M]}{[\mathrm{Xe}]}\frac{1}{\frac{4}{3}x^2+f}. \quad (35)$$

Thus for Rb in Xe where r_2 was given by (19) and $x\simeq 3.1$, we find

$$\frac{1}{\theta_B}=4.1\times10^{-16}\ \mathrm{sec}^{-1}\,\mathrm{cm}^3\,[\mathrm{Rb}]. \quad (36)$$

At a representative number density of $[\mathrm{Rb}]=10^{12}\,\mathrm{cm}^{-3}$ we expect a binary contribution to the relaxation of ^{129}Xe, $\theta_B^{-1}=0.4\times10^{-3}$ sec^{-1}, about 5% of the peak rate at 17 Torr of N_2 but about 13% of the total rate at 100 Torr of N_2 (see Fig. 12). Unfortunately, the electron randomization rates r_2 for K and Cs in xenon gas have not been measured but it is reasonable to guess that they are comparable to the rate for Rb or Na, as discussed in Sec. III, and we shall therefore assume that the contribution of binary collisions to the relaxation of ^{129}Xe in K and Cs vapor is small compared to the relaxation due to van der Waals molecules.

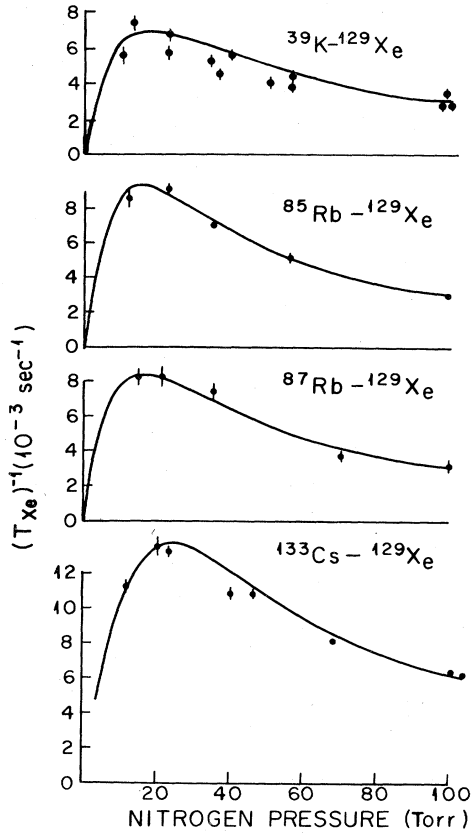

FIG. 12. Summary of the experimentally determined molecular contribution $(T_{Xe})^{-1}$ to the nuclear-spin relaxation rate of ^{129}Xe in cells containing alkali-metal-atom vapors at a number density of 10^{12} cm^{-3}, as deduced from the empirical formulas (30)—(32) and the cell temperatures. Small contributions to $(T_{Xe})^{-1}$ from wall relaxation and electron-randomizing binary collisions have been subtracted to obtain $(T_{Xe})^{-1}$ [see Eq. (39)]. Solid curves are $|q(K,K)|T_K^{-1}$ with $q(K,K)$ given by Eq. (38). Note that the alkali-metal nuclear spin has very little effect on the relaxation of ^{129}Xe, as is evidenced by the data for ^{85}Rb and ^{87}Rb. These data are used to determine the parameters T_K^{-1} and p_0.

For sufficiently high N_2 pressures where $\phi/(2I+1)\ll 1$, one can show that the nuclear-spin destruction probability for ^{129}Xe is

$$|q(K,K)|=\frac{2}{3}\left[\frac{\phi}{(2I+1)x}\right]^2[I(I+1)+\tfrac{3}{4}] \quad (37)$$

for unpolarized alkali-metal atoms but with no restriction on whether x is larger or small than unity. For smaller N_2 pressures where $\phi/(2I+1)\gtrsim 1$ we can express $|q(K,K)|$ as a power series in x^{-2}, and we find

$$|q(K,K)| = \frac{1}{9x^2}(4I^2+4I+3)\frac{\left[\frac{\phi}{2I+1}\right]^2}{1+\left[\frac{\phi}{(2I+1)}\right]^2} + \frac{1}{3(2I+1)}\sum_{fm_f}\left[1-\frac{1}{2x^2}[f(f+1)-m_f^2]\right]\left[\frac{\left[\frac{\phi m_f}{(2I+1)x}\right]^2}{1+\left[\frac{\phi m_f}{(2I+1)x}\right]^2}+\delta m_{f0}\frac{\left[\frac{\phi f(f+1)}{2(2I+1)x^2}\right]^2}{1+\left[\frac{\phi f(f+1)}{2(2I+1)x^2}\right]^2}\right]. \quad (38)$$

Formula (38) is valid only for small values of the expansion parameter x^{-2}.

In summary, we attribute most of the alkali-metal dependent decay rate θ_0^{-1} of ^{129}Xe to relaxation due to van der Waals molecules. A relatively small contribution to θ_0^{-1} from binary alkali-metal—noble-gas collisions is subtracted to obtain the best estimate of the molecule-induced relaxation

$$\frac{1}{T_{Xe}} = \theta^{-1} - r_2\frac{[M]}{[Xe]}\frac{1}{\frac{4}{3}x^2+f} - \frac{1}{T_w}, \quad (39)$$

where as before we approximate the electron randomization rate r_2 for K and Cs by the measured rate $r_2 = 185$ sec^{-1} for Rb.

In Fig. 12 we summarize the measured spin-relaxation rates of ^{129}Xe nuclear spins corrected for wall relaxation and for electron randomizing collisions according to Eq. (39). Alkali-metal-atom vapor densities of 10^{12} atoms/cm^3, as inferred from the empirical formulas (30)—(32), were assumed for Fig. 12. The solid curves in Fig. 12 are the theoretical value $|q(K,K)|T_K^{-1}$ for the relaxation due to van der Waals molecules. The theoretical curves are not very sensitive to the Breit-Rabi parameter x and the value of x was not taken to be a free parameter in the fits of Fig. 12, but x was inferred instead from the ratio of the ^{129}Xe and alkali-metal-atom spin-relaxation rates at high third-body pressures. The two free parameters in the fit were T_K^{-1}, the molecular formation rate per noble-gas atom, and p_0, the characteristic pressure. The value of $|q(K,K)|$, the probability that the ^{129}Xe nuclear spin is destroyed during the molecular lifetime, was taken from Eq. (38).

V. DETERMINATION OF THE BREIT-RABI PARAMETER x FROM THE RATIO OF THE SPIN-RELAXATION TIMES OF THE ALKALI-METAL ATOMS AND THE NOBLE-GAS ATOMS

Let us consider the ratio of the wall-corrected spin-relaxation rate $C[M]$ of the xenon atoms to the slowest spin-relaxation rate of the alkali-metal atoms M,

$$\frac{1}{T_{M,0}} = \gamma_{10} - \frac{\pi^2 D_0\, 760\text{ Torr}}{R^2 P(N_2)} \quad (40)$$

after the effects of optical pumping and spatial diffusion have been eliminated. From (26), (33), and (37) we find that the expected ratio at high N_2 pressures is

$$\frac{\theta_0}{T_{M,0}} = \frac{[Xe]}{[M]}\frac{(x^2+3f/4)}{I(I+1)+\frac{3}{4}} \quad (41)$$

provided that we assume that the Breit-Rabi parameter x is the same for binary collisions as it is for van der Waals molecules and provided that we assume that the contribution of binary collisions to the relaxation of the alkali-metal atoms is given by (21), the value appropriate to the eigenobservable F_z of spin temperature equilibrium. Since we have already shown that the contribution of binary

TABLE II. Data used to determine x for ^{85}Rb^{129}Xe from Eq. (42). Cells all contained 1 Torr of xenon (69 wt. % ^{129}Xe) and the ^{129}Xe relaxation rates were determined at a number density of 10^{12} cm^{-3} according to formula (30). Small contributions of the cell walls to the alkali-metal-atom and noble-gas spin-relaxation rates have been subtracted in accordance with Eqs. (29) and (40).

N_2 pressure in cell	$T_{M,0}$ sec^{-1}	θ_0^{-1} sec^{-1}	$\frac{\theta_0}{T_{M,0}}$
23	346	9.06×10^{-3}	3.82×10^4
35	228	7.13×10^{-3}	3.20×10^4
56	178	5.25×10^{-3}	3.38×10^4
96	124	3.04×10^{-3}	4.06×10^4
Mean value of 56- and 96-Torr cells			3.72×10^4

collisions is small for both $T_{M,0}^{-1}$ and θ_0^{-1}, any modest departure of the alkali-metal eigenobservable from F_z or of the binary value of x from the molecular value will cause a negligible error in our results. We may therefore use (41) to evaluate x^2 from the measured values of θ_0, $T_{M,0}$ and [Xe] and from the alkali-metal number density $[M]$ which we infer from the cell temperature and the saturated vapor-pressure formulas (30)—(32). The explicit expression is

$$x^2=\frac{[M]}{[\mathrm{Xe}]}\frac{\theta_0}{T_{M,0}}[I(I+1)+\tfrac{3}{4}]-\frac{3f}{4}\ . \tag{42}$$

Representative data for $^{85}Rb^{129}Xe$ are shown in Table II. The values of x inferred for ^{129}Xe paired with ^{39}K, ^{85}Rb, ^{87}Rb, and ^{133}Cs are summarized in Table I.

VI. RATIO OF REPOLARIZATION SIGNAL TO PUMPING SIGNAL

In our experiment we detect the nuclear-spin polarization of the noble gas indirectly by observing the "repolarization" signal, i.e., by observing the electronic-spin polarization induced in the alkali-metal atoms by collisions with the nuclear-spin-polarized noble-gas atoms. The magnitude of the repolarization signal depends on many parameters in addition to the magnitude of the nuclear-spin polarization of the noble gas. The intensity, circular polarization, and spectral profile of the probing light; the number densities of the alkali-metal atoms, the noble-gas atoms, and the third-body atoms or molecules; and the spin-relaxing properties of the cell walls can all influence the repolarization signals. The purpose of this section is to show that there is good agreement between the magnitude of the observed repolarization signals and the theoretically expected values.

We measured the repolarization signals with the apparatus sketched in Fig. 13. The cell was optically pumped for several spin-relaxation times of the noble-gas nuclei; a typical pumping time was about 15 min. The pumping light passed through a neutral density (ND) filter, a circular polarizer (CP), the sample cell, and a circular analyzer (CA). At the end of the pump phase the CP was removed from the optical train and a stopwatch was started simultaneously. A radio-frequency magnetic field, 100% square-wave modulated at 10 Hz, was applied to the sample cell at the resonance frequency, 700 KHz/G of the ^{87}Rb atoms. The electron-spin polarization $\langle F_z \rangle$ of the ^{87}Rb was thereby driven to zero for half of the 10-Hz cycle and it was allowed to recover to its repolarized value during the half cycle the rf was off. The recovery time was a few milliseconds and the saturation time in the rf field was even shorter, so the ^{87}Rb polarization was very nearly square-wave modulated also. The modulated ^{87}Rb polarization $\langle F_z \rangle$ modulated the attenuation A of the va-

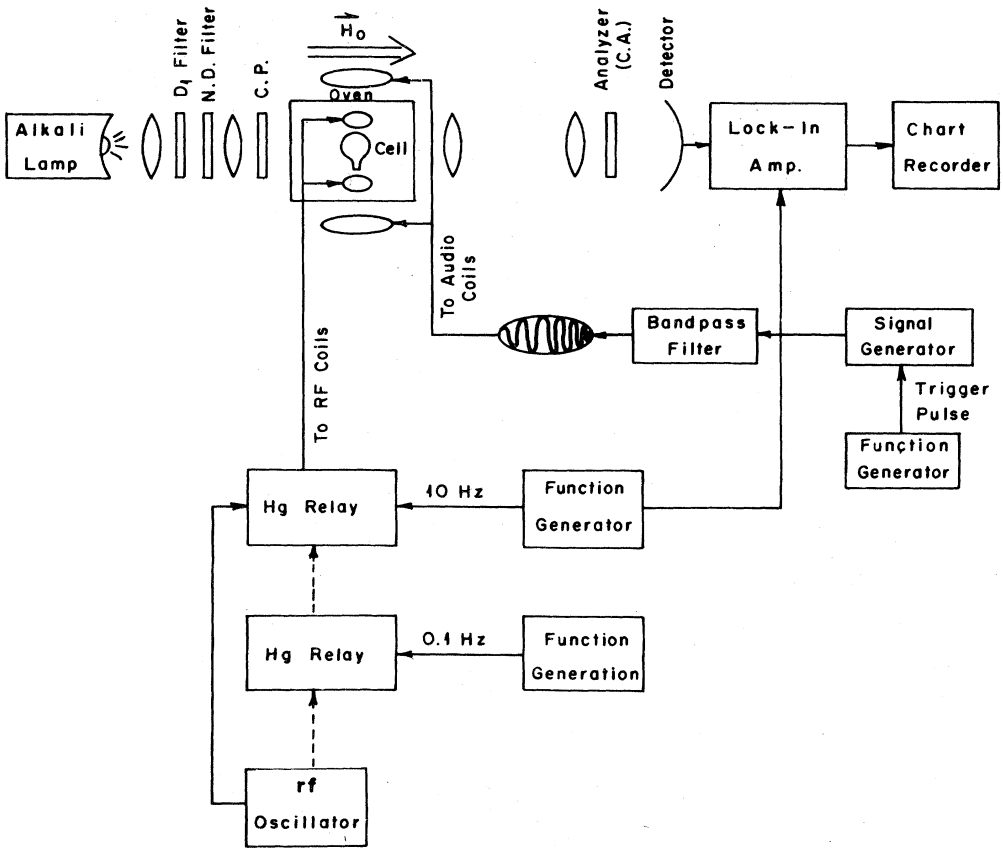

FIG. 13. Apparatus used to measure the ratio of the alkali-metal-atom spin polarization produced by collisions with nuclear-spin polarized ^{129}Xe to the alkali-metal-atom spin polarization during the optical-pumping phase.

por, so the light reaching the detector was square-wave modulated by an amount proportional to the ^{87}Rb spin polarization. The 10-Hz optical signal was detected with a lock-in amplifier referenced to the same 10-Hz modulation frequency. This probe signal decayed slowly because of the relaxation of the ^{129}Xe nuclear polarization which was responsible for the repolarization. To eliminate drifts and offset signals the ^{129}Xe polarization was periodically inverted as described in Sec. IV and the time between the removal of the circular polarizer and the occurrence of the first adiabatic inversion was recorded with the stopwatch. The ^{129}Xe relaxation signal was recorded on chart paper, and by extrapolating the signal amplitude back to the time of removal of the circular polarizer, we were able to infer the initial repolarization signal S_{Xe}.

The circular polarizer was then replaced in the optical train and the much larger signal due to the optically pumped Rb atoms was recorded with exactly the same 10 Hz chopped rf. The rf was turned off completely several times to establish the baseline for the optical pumping signal S_{Rb}. During the recording of the optical pumping signal the adiabatic-inversion pulses were turned off, although we found that this made very little difference to the pumping signal. Data from a representative measurement are shown in Fig. 14.

The ND filter was then replaced by a filter with a different attenuation, the rf was turned off, the cell was pumped for another 15 minutes, and the measurement cycle was repeated as described above. All of the measurements were done at the same cell temperature.

The ratios $S_{\mathrm{Xe}}/S_{\mathrm{Rb}}$ of the repolarization signal to the pump signal was then plotted as a function of the relative light intensity. A representative plot is shown in Fig. 15. It can be seen that the ratio decreases linearly from the zero-light-intensity intercept $(S_{\mathrm{Xe}}/S_{\mathrm{Rb}})_0$. Similar plots were made for other sample cells with different amounts of nitrogen buffer gas but with the same amount, 0.5 Torr, of isotopically enriched Xe gas. We shall subsequently show that except for a correction factor of order unity which accounts for the attenuation of the circular polarizer, the signal ratio $S_{\mathrm{Xe}}/S_{\mathrm{Rb}}$ is equal to the ratio $\langle F_z\rangle_{\mathrm{repol}}/\langle F_z\rangle_{\mathrm{pump}}$, where $\langle F_z\rangle_{\mathrm{pump}}$ and $\langle F_z\rangle_{\mathrm{repol}}$ are the expectation values of the alkali-metal angular momenta during the pump and probe phases, respectively.

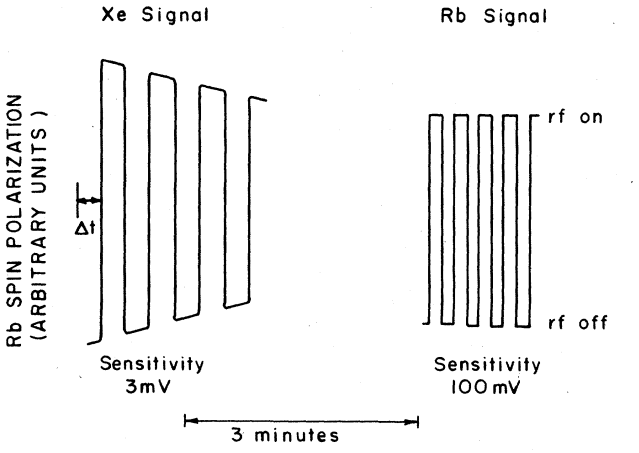

FIG. 14. Sample data (the noise is too small to reproduce) of the repolarization signal and the optical-pumping signal. The initial envelope of the Xe signal is $2S_{\mathrm{Xe}}$ (the factor of 2 comes from the adiabatic inversion) and the envelope of the Rb signal is S_{Rb}.

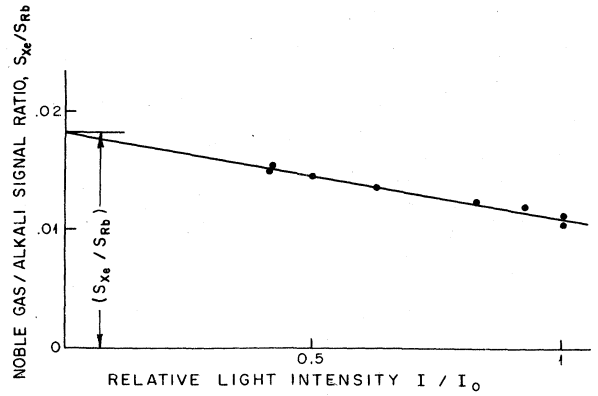

FIG. 15. Dependence of the signal ratio on the intensity of the optical-pumping light. Strong unpolarized light during the probe phase can substantially decrease the magnitude of the repolarization signal.

To interpret these experiments we recall that for weak polarization the attenuation A of the vapor was given by (11). For simplicity we shall neglect the contributions to A of $\langle \vec{I}\cdot\vec{S}\rangle$ and of the two quadrupole observables. This is a good approximation for ^{87}Rb cells probed with ^{87}Rb lamps, since the spectral profile of the lamp is then quasi-broadline and cannot produce $\langle \vec{I}\cdot\vec{S}\rangle$ or the quadrupole observables efficiently[13,16] Furthermore, the attenuation of the light will be relatively insensitive to $\langle \vec{I}\cdot\vec{S}\rangle$, i.e., we expect to find

$$\left|\frac{\partial A}{\partial\langle \vec{I}\cdot\vec{S}\rangle}\right| \ll \left|\frac{\partial A}{\partial\langle f_z\rangle}\right| . \tag{43}$$

Finally, as we mentioned in Sec. III, the relaxation of $\langle \vec{I}\cdot\vec{S}\rangle$ and the quadrupole observables is normally faster than that of $\langle a_z\rangle$ and $\langle b_z\rangle$, and this will further suppress the magnitudes of $\langle \vec{I}\cdot\vec{S}\rangle$ and of the two quadrupole observables relative to the magnitudes of $\langle a_z\rangle$ and $\langle b_z\rangle$. We shall further assume that $\langle a_z\rangle$ and $\langle b_z\rangle$ are well described by the spin temperature approximations,[6] i.e.,

$$\langle f_z\rangle = \frac{f(f+1)(2f+1)}{2(2I+1)[I(I+1)+\frac{3}{4}]}\langle F_z\rangle , \tag{44}$$

where $f=I\pm\frac{1}{2}$. Then (11) can be written as

$$A_\pm = A_0 \pm A_F\langle F_z\rangle , \tag{45}$$

where A_F is a linear combination of $\partial A/\partial\langle a_z\rangle$ and $\partial A/\partial\langle b_z\rangle$.

We will denote the number density of σ_+ photons entering the cell by n_+ and the number density of σ_- photons by n_-. The numbers of σ_+ and σ_- photons emerging from the cell will be $n_+(A_0+A_F\langle F_z\rangle)$ and $n_-(A_0-A_F\langle F_z\rangle)$, respectively. These photon currents

will be attenuated further by factors of a_+ and a_-, respectively, when they pass through the CA. The number density of photons reaching the detector is therefore

$$S=n_+a_+(A_0+A_F\langle F_z\rangle)+n_-a_-(A_0-A_F\langle F_z\rangle) \quad (46)$$

and the signal detected by the lock-in amplifier of Fig. 13 must be proportional to

$$\Delta S=(n_+a_+-n_-a_-)A_F\langle F_z\rangle \ . \quad (47)$$

During the repolarization phase of the measurement the circular polarizer is removed and we will therefore have $n_+=n_-=n_0/2$, where n_0 is the number density of photons in the beam of unpolarized light from the lamp. Then

$$\Delta S_{\rm repol}=\frac{n_0}{2}(a_+-a_-)A_F\langle F_z\rangle_{\rm repol} \ . \quad (48)$$

During the pump-phase measurement we have $n_+=(n_0/2)a_+$ and $n_-=(n_0/2)a_-$. This is so because the polarizer and analyzer are nearly identical and are cut from the same sheet of laminated plastic circular-polarizer material. Thus the pump-phase signal is

$$\Delta S_{\rm pump}=\frac{n_0}{2}(a_+^2-a_-^2)A_F\langle F_z\rangle_{\rm pump} \ . \quad (49)$$

The ratio of the signals is

$$\frac{\Delta S_{\rm repol}}{\Delta S_{\rm pump}}=\frac{1}{a_++a_-}\frac{\langle F_z\rangle_{\rm probe}}{\langle F_z\rangle_{\rm pump}}=\frac{1}{2\bar{a}}\frac{\langle F_z\rangle_{\rm probe}}{\langle F_z\rangle_{\rm pump}} \ . \quad (50)$$

One can easily verify that the fractional attenuation of unpolarized light by the polarizer is

$$\bar{a}=\frac{a_++a_-}{2} \ . \quad (51)$$

For a good polarizer the fractional attenuation is very nearly $\frac{1}{2}$, and for our polarizers we measure

$$\bar{a}=0.44 \ , \quad (52)$$

so the correction factor is $2\bar{a}=0.88$ for our experiments.

The evolution of the noble-gas spin polarization during the pump phase is given by

$$\frac{d}{dt}\langle K_z\rangle=-\frac{1}{T_w}\langle K_z\rangle+\frac{1}{T_K}[q(K,K)\langle K_z\rangle+q(K,F)\langle F_z\rangle] \quad (53)$$

which has the steady-state solution

$$\langle K_z\rangle_0=\frac{q(K,F)\langle F_z\rangle_{\rm pump}}{\frac{T_K}{T_w}+|q(K,K)|} \quad (54)$$

since $q(K,K)<0$.

If we ignore the effects of spatial diffusion and other small relaxation mechanisms (but not spin exchange, which has no effect on $\langle F_z\rangle$) we may describe the evolution of the alkali-metal-atom spin polarization by

$$\frac{d}{dt}\langle F_z\rangle=-\frac{1}{T_{\rm opt}}\langle F_z\rangle+\frac{1}{T_F}[q(F,F)\langle F_z\rangle+fq(F,K)\langle K_z\rangle] \ , \quad (55)$$

where $(T_{\rm opt})^{-1}$ is the spin-depolarization rate due to the unpolarized probe light. The value of $\langle K_z\rangle$ decreases very slowly with time compared to the characteristic time $T_F\simeq 10^{-3}$ sec, so we may write the quasi-steady-state solution to (55) as

$$\langle F_z\rangle_{\rm repol}=\frac{fq(F,K)\langle K_z\rangle}{\frac{T_F}{T_{\rm opt}}+|q(F,F)|} \quad (56)$$

since $q(F,F)<0$.

Thus, we expect the ratio of the alkali-metal-atom spin polarization at the beginning of the repolarization measurement to the pump-phase polarization to be

$$\frac{\langle F_z\rangle_{\rm repol}}{\langle F_z\rangle_{\rm pump}}=\frac{fq(F,K)q(K,F)}{\left[\frac{T_F}{T_{\rm opt}}+|q(F,F)|\right]\left[\frac{T_K}{T_w}+|q(K,K)|\right]} \ . \quad (57)$$

In the limit of low light intensity, $T_{\rm opt}\to\infty$, and we may rewrite (57) as

$$r=\frac{fq(F,K)q(K,F)}{q(F,F)q(K,K)}=\frac{\frac{1}{T_w}+\frac{1}{T_K}|q(K,K)|}{\frac{1}{T_K}|q(K,K)|}\left[\frac{\langle F_z\rangle_{\rm repol}}{\langle F_z\rangle_{\rm pump}}\right]_0 \ . \quad (58)$$

The correction factor

$$\frac{\frac{1}{T_w}+\frac{1}{T_K}|q(K,K)|}{\frac{1}{T_K}|q(K,K)|}=\frac{\frac{1}{T_w}+C[{\rm Rb}]}{C[{\rm Rb}]} \quad (59)$$

can be determined experimentally from data like those of Fig. 11, and in view of (50) we expect to find

$$r=\frac{fq(F,K)q(K,F)}{q(F,F)q(K,K)}=\frac{\frac{1}{T_w}+C[{\rm Rb}]}{C[{\rm Rb}]}2\bar{a}\left[\frac{\Delta S_{\rm repol}}{\Delta S_{\rm pump}}\right]_0 \ . \quad (60)$$

Equation (60) gives two expressions for the repolarization ratio r: a purely theoretical formula in the middle involving the spin-transfer coefficients $q(F,K)$, etc., and on the right-hand side, an experimental ratio corrected for the effects of ^{129}Xe wall relaxation (a factor slightly larger than 1) and for the polarizer attenuation ($2\bar{a}=0.88$, a factor slightly less than 1). The experimental and theoretical values of r are compared in Fig. 16. Note that there are no adjustable parameters in Fig. 16. The Breit-Rabi parameter x and the characteristic pressure p_0 which go into the evolution of the spin-transfer coefficients [e.g., see (38)

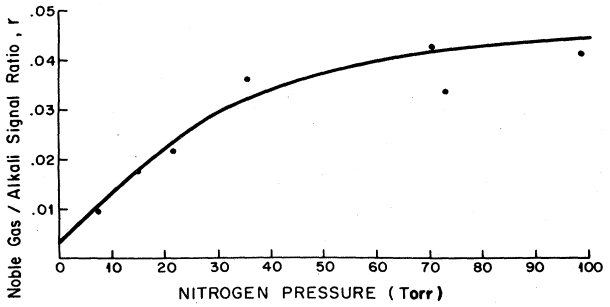

FIG. 16. Dependence of the measured ratio of the repolarization signal to the pump-phase signal on the third-body (N_2) pressure in the sample cells. The ratio was corrected for the attenuation of the polarizers in Fig. 13 and for the wall relaxation of the ^{129}Xe according to Eq. (60). The signal ratio is severely depressed at low nitrogen pressures. It is therefore difficult to observe repolarization signals at low nitrogen pressures. The solid curve is drawn according to Eq. (60) with a distribution of the rotational angular momentum N taken into account. There are no free parameters for the solid curve.

and (6)] were determined from the independent data of Secs. III—V. We should also mention that the number density of ^{129}Xe need not be known precisely for the ratio measurements since additional xenon decreases the pump and repolarization signals by the same factor. The ratio measurement is also not affected by any miscalibration of the Rb vapor-pressure curves versus temperature as long as the same curves are used to deduce the correction factor (59) for ^{129}Xe wall relaxation from data like those of Fig. 11.

We have not made quantitative measurements of the repolarization ratios for ^{85}Rb or ^{133}Cs because we do not feel that the ratio measurements are as effective a way to measure the parameters x and p_0 as the methods based on analyzing the spin-decay transients of the alkali-metal atoms and the xenon nuclei, which were discussed in Secs. III—V. One problem with the ratio measurements is the contribution of observables other than $\langle F_z \rangle$ to the attenuation of the light. The influence of these observables is nearly eliminated when we measure the slowest spin-relaxation transient of alkali-metal atoms as described in Sec. III. However, $\langle \vec{I} \cdot \vec{S} \rangle$, the quadrupole observables, and the more rapidly relaxing dipole observable all contribute somewhat to the optical pumping signal and repolarization signal described in this section. This is an especially annoying problem with ^{133}Cs, where quadrupole polarization is easily generated and observed because of the relatively large excited-state hyperfine structure of the ^{133}Cs atom. The large contribution of quadrupole observables to the optical pumping signals of ^{133}Cs was first pointed out by Bouchiat *et al.*[14] We can therefore expect to find somewhat poorer quantitative agreement between theoretically calculated and experimentally measured values of the repolarization ratio for ^{133}Cs than for the ^{87}Rb data shown in Fig. 16. The ratio measurements should be very reliable for ^{39}K, with its small hyperfine-structure intervals, and experimental measurements of the ratio for ^{39}K, similar to those described above for ^{87}Rb, are well fit by the parameters of Table I.

VII. *RC* NETWORK MODEL

The motivation for many of the experiments described in the earlier sections of this paper can be understood with the aid of the *RC* network model illustrated in Fig. 17. As was shown in Ref. 6, the spin-polarized alkali-metal atoms and noble-gas atoms can be thought of as two capacitors with values,

$$C_M = \Omega[M]\langle F^2 - F_z^2 \rangle \tag{61}$$

and

$$C_{\mathrm{Xe}} = f\Omega[\mathrm{Xe}]\langle K^2 - K_z^2 \rangle , \tag{62}$$

on which the angular momentum charges

$$Q_M = \Omega[M]\langle F_z \rangle \tag{63}$$

and

$$Q_{\mathrm{Xe}} = f\Omega[\mathrm{Xe}]\langle K_z \rangle \tag{64}$$

are stored. Here Ω is the volume of the cell, so $\Omega[M]$ and $\Omega[\mathrm{Xe}]$ are the total number of alkali-metal and xenon atoms in the sample cell. The quantities

$$2\langle F^2 - F_z^2 \rangle = 1 + \tfrac{4}{3}I(I+1) + \cdots \tag{65}$$

and

$$2\langle K^2 - K_z^2 \rangle = \tfrac{4}{3}K(K+1) + \cdots \tag{66}$$

which occur in (61) and (62) play much the same role as dielectric constants for ordinary electrical capacitors. They account for the fact that atoms with high-spin quantum numbers can store more angular momentum than atoms with low spin quantum numbers. Corrections to the "paramagnetic constants" at high spin polarization are denoted by centered ellipses in (65) and (66) and are discussed in detail in Ref. 6.

The optical pumping lamp or laser is represented by a battery attached to the alkali-metal capacitor. The emf of the battery is

$$V_{\mathrm{opt}} = s_z , \tag{67}$$

where s_z is the mean spin of the pumping photons ($s_z = \pm 1$ for $\sigma_\pm$ light). The internal resistance R_{opt} of the battery is defined by

$$\frac{1}{R_{\mathrm{opt}}} = \frac{\Omega[M]R}{2} , \tag{68}$$

where R is the mean optical-pumping rate of the light source. That is, (68) implies that the optical admittance is one-half of the number of photons absorbed per second by the alkali-metal atoms in the cell. More details about the physical assumptions leading to (67) and (68) can be found in Ref. 6.

The capacitor C_M is shunted to ground by the spin-rotation resistor R_{sr} defined by

$$\frac{1}{R_{\mathrm{sr}}} = \frac{1}{T_0}\frac{2}{3}\left[\frac{\gamma N \tau}{(2I+1)}\right]^2 \langle F^2 - F_z^2 \rangle , \tag{69}$$

where the global molecular-formation rate in the sample cell is given by

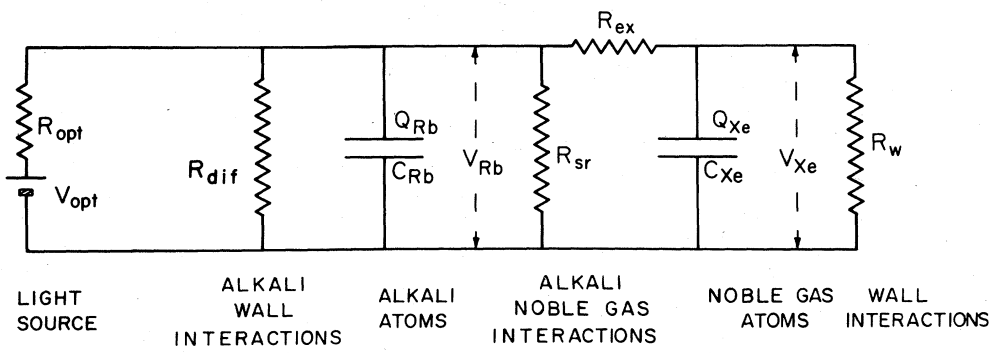

FIG. 17. *RC* network model for alkali-metal—noble-gas spin exchange. Angular momentum is analogous to electrical charge, and the alkali-metal and noble-gas atoms in which the angular momentum is stored are represented by capacitors. The optical-pumping light is equivalent to a battery whose emf is the mean spin of the pumping photons.

$$\frac{1}{T_0}=\frac{\Omega[M]}{T_F}=\frac{\Omega[\mathrm{Xe}]}{T_K} . \tag{70}$$

The capacitors C_M and C_{Xe} are coupled by the exchange resistor R_{ex} defined by

$$\frac{1}{R_{\mathrm{ex}}}=\frac{f}{T_0}\left[\frac{\alpha\tau}{(2I+1)}\right]^2\langle F^2-F_z^2\rangle\langle K^2-K_z^2\rangle . \tag{71}$$

The xenon capacitor is shunted to ground through the wall resistor R_w, which is defined in terms of the empirically determined wall-relaxation time T_w by

$$\frac{1}{R_w}=\frac{C_{\mathrm{Xe}}}{T_w} . \tag{72}$$

The alkali-metal capacitor is shunted to ground by an analogous diffusion resistor defined by

$$\frac{1}{R_{\mathrm{dif}}}=C_{\mathrm{Xe}}\gamma_D , \tag{73}$$

where the slowest diffusion rate γ_D was defined in (24). The voltages on the capacitors are

$$V_{\mathrm{Rb}}=\frac{Q_M}{C_M}=\frac{\langle F_z\rangle}{\langle F^2-F_z^2\rangle} \tag{74}$$

and

$$V_{\mathrm{Xe}}=\frac{Q_{\mathrm{Xe}}}{C_{\mathrm{Xe}}}=\frac{\langle K_z\rangle}{\langle K^2-K_z^2\rangle} . \tag{75}$$

Under the conditions of spin temperature equilibrium, described more fully in Ref. 6, the magnitudes of the voltages in (74) and (75) never exceed unity, the value corresponding to 100% positive or negative polarization.

From inspection of (48), (49), and the equations which follow from (11), it can be seen that most of our experiments are designed to detect $\langle F_z\rangle$ or in view of Eq. (63), the charge Q_M on the alkali-metal capacitor. We detect the charge Q_{Xe}, or equivalently the nuclear-spin polarization of the xenon atoms, indirectly through the charge induced on the alkali-metal capacitor by the voltage V_{Xe}.

The measurement of the slowest spin-relaxation transient of the alkali-metal atoms, which was described in Sec. III, can be thought of as an experiment to determine the *RC* time constant of the alkali-metal capacitor. This time constant is dominated by the leakage of charge off of C_M through the relatively small spin-rotation resistor R_{sr} to ground. Some shortening of the time constant is caused by discharge through the internal resistance R_{opt} of the battery, and this parasitic leakage is eliminated by the extrapolation to zero light intensity illustrated in Fig. 7. The leakage through the diffusion resistor R_{dif} is small at high nitrogen pressures and is accounted for in Eq. (28). The leakage through R_{ex} to ground is accounted for by the term proportional to x^{-2} in Eq. (26).

The measurement of the ^{129}Xe spin-relaxation transient described in Sec. IV can be thought of as an experiment to determine the *RC* time constant of the xenon capacitor C_{Xe}. The charge on C_{Xe} leaks to ground through the wall resistor R_w and through the series combination of the relatively large exchange resistor R_{ex} and the much smaller ($\lesssim 5\%$ R_{ex}) parallel combination of R_{sr}, R_{dif}, and R_{opt}. In analyzing the data of Secs. IV and V we have made the simplifying assumption that because of the low alkali-metal spin polarization during the ^{129}Xe relaxation transient the left side of R_{ex} in Fig. 17 is essentially at ground potential.

The ^{129}Xe nuclear spins relax about 10^5 times more slowly than the alkali-metal-atom spins according to Figs. 8 and 12. This is because the xenon capacitor C_{Xe} is about 10^4 times larger than the alkali-metal capacitor C_M due to the much larger ($\sim 3\times 10^4$) number of xenon atoms than alkali-metal atoms, and also because the leakage resistor for C_{Xe}, R_{ex} is about a factor of 10 larger than R_{sr}, the leakage resistor for C_M. However, C_M is increased relative to C_{Xe} because of the large contribution of the nuclear spin I of the alkali-metal atom to the paramagnetic constant of C_M. This can be clearly seen from Fig. 8, where the measured time constant for ^{85}Rb ($I=\frac{5}{2}$) relaxation is about a factor of 2 longer than the time constant for ^{87}Rb ($I=\frac{3}{2}$) relaxation.

The repolarization ratio measurements described in Sec. VI can be thought of as experiments to determine the magnitude of the "voltage divider" which consists of the resistors R_{ex} and R_{sr} connected in series between C_{Xe} and ground. The high-pressure asymptote $r\simeq 0.05$ shown in Fig. 16 is the voltage-divider ratio $R_{\mathrm{sr}}/(R_{\mathrm{sr}}+R_{\mathrm{ex}})$. The

extrapolation of Fig. 15 is designed to eliminate the shunting effect of R_{opt} across R_{sr}.

Finally, we should note that the RC network of Fig. 17 is appropriate to high N_2 pressures where $\phi \ll 1$ and $q(K,K) = -q(K,F)$. Under these conditions very little spin transfer among F, N, and K occurs during each molecular lifetime. For lower N_2 pressures where $\phi \gtrsim 1$, very substantial changes of F and K can occur during each molecular lifetime, and much of the atomic and nuclear spin angular momentum is transferred to the rotational angular momentum N of the molecule. Then the RC network of Fig. 17 should be modified to include an additional shunt resistor across C_{Xe}. This new shunt resistor as well as the resistors R_{ex} and R_{sr} can be defined in a straightforward way in terms of the spin coupling coefficients of Eqs. (1) and (2).

VIII. CONCLUSIONS

The data of Fig. 10 demonstrate that excellent ^{129}Xe nuclear-spin polarization signals can be observed in K, Rb, and Cs alkali-metal-atom vapors. Adrianov[30] *et al.* have already reported that ^{133}Cs is comparable to the Rb isotopes as a spin-exchange partner for ^{129}Xe, but they reported no systematic studies of the dependence of the exchange rate on third-body pressure. The quantitative data of Table I, the main results of the work described in this paper, show that the parameters x, p_0, and Z are similar in magnitude for all three alkali metals.

We are unable to deduce absolute values for the spin-rotation constant γN and the spin-exchange constant α from the spin-relaxation data described in this paper. Independent magnetic-decoupling experiments[31] are low being carried out in our laboratory to establish the magnitude of γN.

The dependence of the relaxation rates on third-body (N_2) pressure (see Figs. 8 and 12) is characteristic of three-body processes where the relaxation rate is the product of a molecular-formation rate T_K^{-1} or T_F^{-1} and a spin-destruction probability $|q(K,K)|$ or $|q(F,F)|$, as indicated in Eq. (33) or (8). At low N_2 pressures the molecular lifetimes are so long that $|q(K,K)|$ and $|q(F,F)|$ are independent of pressure and equal to their saturated values, $\frac{2}{3}$, which is the probability that $\vec{N}$ will be perpendicular to the external magnetic field when a van der Waals molecule is formed. The relaxation rates are therefore proportional to the molecular-formation rates or the N_2 pressure.

For very high N_2 pressure the spin-destruction probabilities must be proportional to the square of the molecular lifetime or inversely proportional to the square of the N_2 pressure. The relaxation rate at high N_2 pressure must therefore be inversely proportional to the N_2 pressure. The noble-gas and alkali-metal-atom spin-relaxation rates attain their peak values at pressures on the order of $p_0/3x$ and $p_0/(2I+1)$, respectively.

The overall precision of these experiments is not very high, especially since we have relied on the saturated vapor-pressure formulas (30)—(32) to estimate the alkali-metal number density from the cell temperature. A temperature measurement error of 1 °C corresponds to a vapor-density error of 5—10 %. As we discussed in Sec. IV, published vapor-pressure curves for Rb differ by more than a factor of 2 in the temperature range of our experiments.

We also note that the value $x = 3.1$ given in Table I for Rb ^{129}Xe is substantially smaller than the value $x = 4.1$ estimated in earlier work from this laboratory.[31] The reason for this discrepancy is not clear although it may be at least partially due to inadequate mixing of the Xe, N_2, and He gases used in the sample cells of Ref. 31. Those cells were prepared without the stopcock C of Fig. 2 and therefore much longer times were required to ensure complete interdiffusion of the gases. In the analysis of the data of Ref. 31 a crucial assumption was that each absorbed σ_+ photon deposited $\hbar/2$ units of angular momentum in the vapor. The spin-transfer efficiency from photons to alkali-metal atoms needs more study. Finally, the NMR data of Ref. 29 were calibrated by comparison to a rather noisy signal from distilled water. We believe that the value of $x = 3.1$ obtained for RbXe in this experiment is more reliable than the earlier value $x = 4.1$ because the same value was measured for both ^{87}Rb and ^{85}Rb and because the ratio data of Sec. VI are in good agreement with the theory. The repolarization ratio is very sensitive to the value of x. The data for ^{133}Cs were less extensively checked.

From a practical point of view the data of Table I indicate that K vapor might be a more useful spin-exchange medium for noble gases than Rb or Cs vapor. This is because the 769.9-nm D_1 absorption line of K atoms is near the peak of the gain curves for oxazine or LD700 dyes. Dye-laser operation is less efficient at the 794.7- and 894.4-nm D_1 lines of Rb and Cs. The larger value of x for potassium compared to cesium or rubidium is a disadvantage since of the alkali-metal-atom spin angular momentum lost during a collison, a fraction, $3/4x^2$, goes into the nuclear spin K of the noble gas; the remainder is lost to the rotational angular momentum N. However, for laser pumping at high cell temperatures the alkali-metal-atom spins are destroyed mainly by alkali-metal-atom—alkali-metal-atom collisions[21] rather than by spin-rotation interactions in alkali-metal—noble-gas van der Waals molecules. The important physical quantity is therefore not the value of x but the relative size of the alkali-metal-atom—noble-gas spin-exchange rate and the alkali-metal-atom—alkali-metal-atom spin-destruction rate, a rate which has been measured[21] only for Cs. Because of the smaller value of the nuclear charge of K atoms compared to Cs atoms, the alkali-metal-atom—alkali-metal-atom spin-destruction rates, which can be traced back to spin-orbit interactions, may be much smaller for K atoms than for Cs atoms or Rb atoms.

ACKNOWLEDGMENTS

This work was supported by the U. S. Air Force Office of Scientific Research under Grant No. AFOSR-81-0104-C.

[1]M. A. Bouchiat, T. R. Carver, and C. M. Varnum, Phys. Rev. Lett. **5**, 373 (1960); R. L. Gamblin and T. R. Carver, Phys. Rev. **138**, A946 (1965).
[2]R. M. Herman, Phys. Rev. **137**, A1062 (1965).
[3]B. C. Grover, Phys. Rev. Lett. **40**, 391 (1978).
[4]C. H.Volk, T. M. Kwon, and J. G. Mark, Phys. Rev. A **21**, 1549 (1980).
[5]N. D. Bhaskar, W. Happer, and T. McClelland, Phys. Rev. Lett. **49**, 25 (1982).
[6]W. Happer, E. Miron, S. Schaefer, D. Schreiber, W. A. van Wijngaarden, and X. Zeng, Phys. Rev. A **29**, 3092 (1984).
[7]M. A. Bouchiat, J. Brossel, and L. C. Pottier, J. Chem. Phys. **56**, 3703 (1972); C. C. Bouchiat, M. A. Bouchiat, and L. C. L. Pottier, Phys. Rev. **181**, 144 (1969).
[8]H. Kopferman, *Nuclear Moments* (Academic, New York, 1968).
[9]N. Ramsey, E. Miron, X. Zeng, and W. Happer, Chem. Phys. Lett. **102**, 340 (1983).
[10]X. Zeng, E. Miron, W. A. van Wijngaarden, D. Schreiber, and W. Happer, Phys. Lett. **96A**, 191 (1983).
[11]The isotopically enriched sample of Xe gas used in this work was purchased from the Isotec Corporation of Centerville, Ohio.
[12]W. Happer, Rev. Mod. Phys. **44**, 169 (1972).
[13]M. A. Bouchiat, J. Phys. (Paris) **24**, 379 (1963); **24**, 611 (1963).
[14]M. A. Bouchiat and F. Grossetete, J. Phys. (Paris) **27**, 353 (1966).
[15]F. A. Franz and C. Volk, Phys. Rev. A **14**, 1711 (1976).
[16]B. S. Mathur, H. Y. Tang, and W. Happer, Phys. Rev. A **2**, 648 (1970).
[17]N. D. Bhaskar, J. Camparo, W. Happer, and A. Sharma, Phys. Rev. A **23**, 3048 (1981).
[18]Mei-Yin Hou, Bing-Ying Cheng, and Rui Ju, Chin. Phys. Lett. **1**, 57 (1984).
[19]K. Ernst and E. Strumia, Phys. Rev. **170**, 48 (1968).
[20]H. M. Gibbs, and R. J. Hull, Phys. Rev. **153**, 132 (1967).
[21]N. D. Bhaskar, J. Pietras, J. Camparo, and W. Happer, Phys. Rev. Lett. **44**, 930 (1980).
[22]F. A. Franz and C. E. Sooriamoorthi, Phys. Rev. A **8**, 2390 (1973).
[23]N. D. Bhaskar, M. Hou, M. Ligare, B. Suleman, and W. Happer, Phys. Rev. A **22**, 2710 (1980).
[24]F. Masnou-Seeuws and M. A. Bouchiat, J. Phys. (Paris) **28**, 406 (1967).
[25]C. Smithells, *Metals Reference Handbook* (Butterworths, London, 1962).
[26]M. A. Bouchiat and J. Brossel, Phys. Rev. **147**, 41 (1966).
[27]T. Killian, Phys. Rev. **27**, 578 (1926).
[28]A. N. Nesmeyanov, *Vapor Pressure of the Elements* (Academic, New York, 1963).
[29]C. H. Volk, T. M. Kwon, J. G. Mark, Y. B. Kim, and J. C. Woo, Phys. Rev. Lett. **44**, 136 (1980).
[30]B. A. Andrianov, V. M. Lopatin, P. S. Ovcharenko, Yu. M. Petukhov, and E. M. Sychugov, Pis'ma Zh. Tekh. Fiz. **7**, 848 (1981) [Sov. Tech. Phys. Lett. **7**, 363 (1981)].
[31]N. D. Bhaskar, W. Happer, M. Larsson, and X. Zeng, Phys. Rev. Lett. **50**, 105 (1983).